

MEDICAL IMAGING MODALITIES: MAGNETIC RESONANCE IMAGING

Like X-ray computed tomography (CT), magnetic resonance imaging (MRI) is a tomographic imaging method that produces 3-D images of the human body, but it is not based on the transmission of external radiation for imaging. MRI uses the nuclear magnetic resonance (NMR) property of selected nuclei of the matter of the object. MRI provides high-resolution images with excellent soft-tissue contrast superior to X-ray CT because of the underlying physics of the imaging process. It is difficult to produce images with good soft-tissue contrast, and information about changes in physiological parameters (such as oxygenation level) and functions (such as diffusion and perfusion) through X-ray CT because X rays do not provide measurable differentiation (leading to contrast in the image) for them. MRI uses selected nuclei, such as hydrogen protons, available in the body for NMR, which produces an electromagnetic signal for imaging. Thus, differentiation (or contrast) in the MRI signal is based on the difference of hydrogen protons in the tissue and physiological structures. Hydrogen protons are readily available in water and other fluids in the body and vary in density within a tissue if its chemical composition changes, providing the basis for better imaging. MRI is a powerful modality for imaging anatomical structures as well as biochemical properties based on physiological function, including blood flow and oxygenation (1–3).

The principle of NMR was independently explained by Felix Bloch and Edward Purcell in 1946. Later, Paul Lauterbur used the NMR principle in MRI to obtain physical and chemical properties based images of an object (2, 3). Paul Lauterbur and Sir Peter Mansfield were jointly awarded Nobel Prize in Medicine in 2003 for their discoveries concerning MRI. Today, MRI techniques are used in multidimensional imaging of the human body, providing both structural and physiological information about internal organs and tissues (1–3).

Magnetic resonance imaging is a complex multidimensional imaging modality that produces extensive amounts of data. Imaging methods and techniques applied in signal acquisition allow reconstruction of images with multiple parameters that represent various physical and chemical properties of the matter of the object. Figure 5.1 shows three images of the same cross-section of a human brain with different

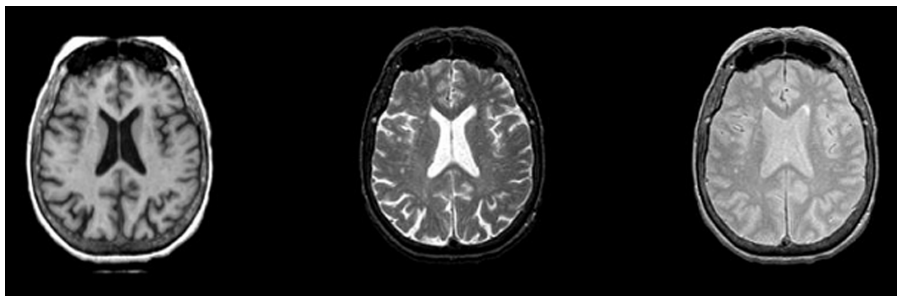


Figure 5.1 MR images of a selected cross-section that are obtained simultaneously using a specific imaging technique. The images show (from left to right), respectively, the T_1 -weighted, T_2 -weighted and the spin-density property of the hydrogen protons present in the brain.

parameters: T_1 weighted, T_2 weighted, and spin density (also called proton density). These images are reconstructed from the data generated through specialized imaging techniques called pulse sequences. MRI pulse sequences provide signal timing and spatial encoding of the object space for data acquisition. Recent advances in MRI include MR spectroscopy, functional (fMRI), and diffusion tensor imaging (DTI) modalities that have sophisticated means of obtaining localized characteristic information about the physiological behavior of the human organ or tissue. For example, a sequence of fMRI images of the brain can show the changes in blood flow or oxygenation levels in the auditory cortex when a signal for auditory stimulation is presented to a subject. A significant advantage of MRI is that it can create any directional cross-sectional images along with multidimensional image sequences without making any physical changes in the instrumentation during imaging. Another advantage of MRI is fast signal acquisition (of the order of a fraction of a second) with a very high spatial resolution in the range of a millimeter to one-hundredth of a millimeter. However, in practice, due to the limitations of instrumentation used in data acquisition methods, these parameters are realized with a lower range to maintain a reasonable signal-to-noise ratio (SNR) for acceptable image quality.

5.1. MRI PRINCIPLES

The basic objective of MR imaging is to map the spatial location and associated properties of specific nuclei or protons present in the object being imaged. The hydrogen proton is the most common form of nuclei used in MRI. Figure 5.1 shows three images displaying three properties of hydrogen nuclei (protons) mapping their spatial locations present in a selected cross-section of the brain. These properties are the spin-lattice relaxation time T_1 , spin-spin relaxation time T_2 , and the spin density ρ . These properties and their significance in diagnostic radiology are described later in this chapter. The high-resolution anatomical information can be seen with different contrast features in Figure 5.1.

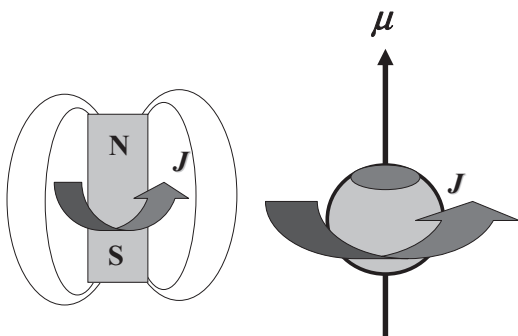


Figure 5.2 Left: A tiny magnet representation of a charged proton with angular moment, J . Right: A symbolic representation of a charged proton with angular moment, J , and a magnetic moment, μ .

The principle of NMR is based on the quantum properties of nuclei and protons. A fundamental property of nuclei with odd atomic weight and/or odd atomic numbers is the possession of angular moment, generally called spin. These protons carry an electric charge and spin around their axes (Fig. 5.2). Because of the spinning, the charged protons create a magnetic field around them and thus act like tiny magnets possessing both angular moment and magnetic moment. The magnetic moment is proportional to the spin angular moment and is related through a constant, called the gyromagnetic ratio, a quantum property of the proton. Thus, the relationship between the spin angular moment, \vec{J} , and the magnetic moment, $\vec{\mu}$, is described by

$$\vec{\mu} = \gamma \vec{J} \quad (5.1)$$

where γ is a gyromagnetic ratio defined in megahertz/Tesla.

A hydrogen atom, for example, has only one proton in its nucleus and thus exhibits the property of nuclear spin. Its gyromagnetic ratio is 42.58 MHz/T, providing a corresponding magnetic moment that is excellent for imaging the human body under an external magnetic field of 0.5 to 1.5 T. The hydrogen proton is also an important in NMR imaging of the human body because of its presence in water molecules, which are available in abundance in the body. However, other protons that exhibit the NMR phenomenon and are available in the body for MRI include ^{13}C , ^{19}F , and ^{31}P (1–5).

The spinning protons with both angular and magnetic moment possess a specific spin quantum number that characterizes their orientations and corresponding energy levels with or without the presence of an external magnetic field. In the absence of an external magnetic field, the direction of the magnetic moments of spinning protons or nuclei is completely random. In the presence of an external magnetic field, the magnetic moments of nuclei result in a nuclear paramagnetic polarization with specific orientations and energy levels as characterized by their spin quantum number. Also, the interaction between the magnetic moment of nuclei with the external magnetic field causes the spinning nuclei to precess, similar to the wobbling of a spinning top, under the gravitational field. The precession of a

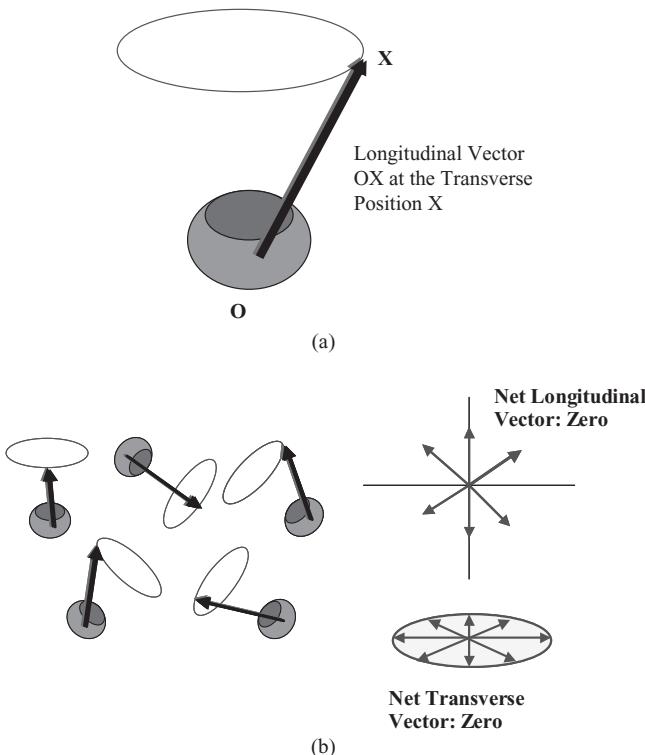


Figure 5.3 (a) A symbolic representation of a proton with precession that is experienced by the spinning proton when it is subjected to an external magnetic field. (b) The random orientation of protons in matter with the net zero vector in both longitudinal and transverse directions.

spinning proton (or nucleus) is shown in Figure 5.3. The spin quantum number of hydrogen proton (${}^1\text{H}$) and other nuclei such as ${}^{13}\text{C}$, ${}^{19}\text{F}$, and ${}^{31}\text{P}$ is $\frac{1}{2}$. When such nuclei are placed under an external magnetic field, they are aligned either along the external magnetic field or against the magnetic field. The energy level of nuclei aligning themselves along the external magnetic field is lower than the energy level of nuclei aligned against the external magnetic field. Upon establishing a thermal equilibrium in the presence of an external magnetic field, the total number of nuclei aligned along the external magnetic field is slightly larger than the number of nuclei aligned against the external magnetic field. This results in a net magnetization vector in the direction of the external magnetic field as shown in Figure 5.4. However, the precession phase is still random, providing a net zero vector in the transverse direction.

Using the principle of classical mechanics, the torque generated by the interaction of magnetic moment of a proton and the external magnetic field is equal to the rate of change of angular momentum and can be given by the equation of motion for isolated spin as (1–3)

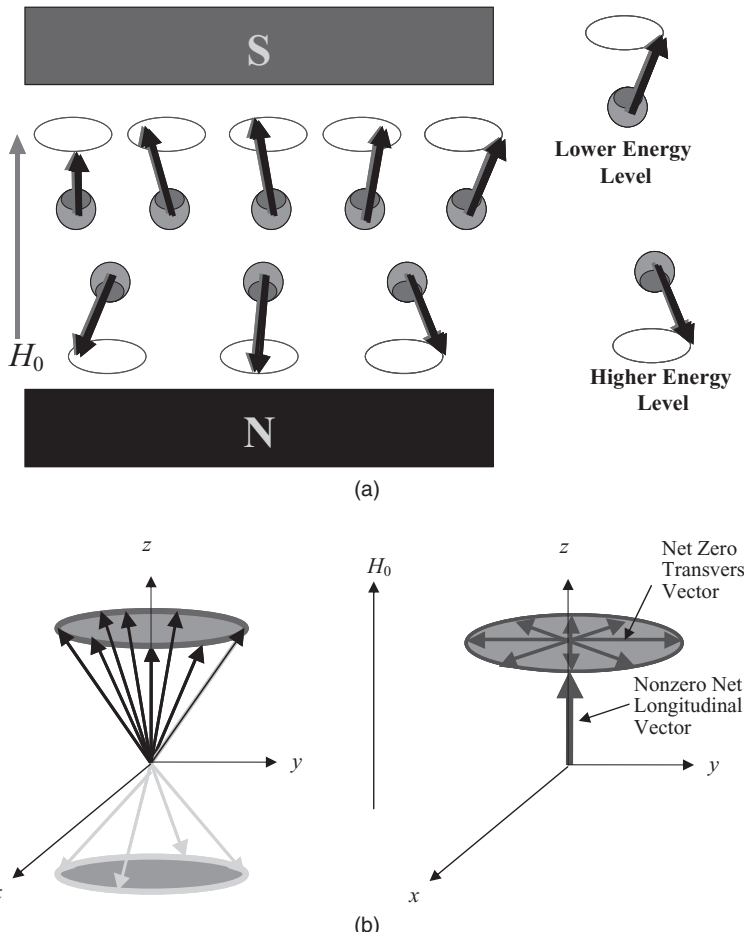


Figure 5.4 (a) Nuclei aligned under thermal equilibrium in the presence of an external magnetic field. (b) A nonzero net longitudinal vector and a zero transverse vector provided by the nuclei precessing in the presence of an external magnetic field.

$$\frac{d\vec{J}}{dt} = \bar{\mu} \times \vec{H}_0 = \bar{\mu} \times H_0 \vec{k}. \quad (5.2)$$

Since $\bar{\mu} = \gamma \vec{J}$, the derivative equation can be written as

$$\frac{d\bar{\mu}}{dt} = \gamma \bar{\mu} \times H_0 \vec{k} \quad (5.3)$$

where H_0 is the strength of the external magnetic field and \vec{k} is the unit vector in z -direction with $\vec{H}_0 = H_0 \vec{k}$.

The solution of the above equation leads to an important relationship that provides the angular frequency, ω_0 , of nuclear precession as

$$\omega_0 = \gamma H_0 \quad (5.4)$$

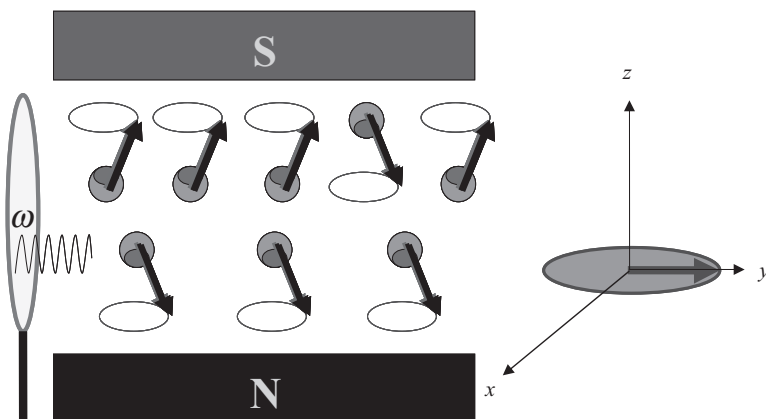


Figure 5.5 The 90-degree pulse causing nuclei to precess in phase with the longitudinal vector shifted clockwise by 90 degrees as a result of the absorption of RF energy at the Larmor frequency.

The above relationship in Equation 5.4 is also known as the Larmor equation. Thus, the precession frequency depends on the type of nuclei with a specific gyromagnetic ratio and the intensity of the external magnetic field. This is the frequency on which the nuclei can receive the radio frequency (RF) energy to change their states to exhibit NMR. The excited nuclei return to the thermal equilibrium through a process of relaxation, emitting energy at the same precession frequency, ω_0 .

During NMR, the nuclei can receive energy to move from the lower-energy state to the higher energy state. In other words, upon receiving the RF energy at the Larmor frequency, the nuclei spinning with an orientation along the external magnetic field can flip to an orientation against the magnetic field. As a result of the change in the orientation of the excited nuclei, the net longitudinal vector is no longer in the direction of the external magnetic field (z -direction). It starts moving away from the z -direction. An RF energy pulse required to shift the longitudinal vector by 90 degrees is called the “90-degree pulse.” Upon receiving energy at the Larmor frequency, the transverse vector also changes as nuclei start to precess in phase. After the completion of the 90-degree pulse, all of the nuclei precess in phase and therefore form a net nonzero transverse vector that rotates in the x - y plane perpendicular to the direction of the external magnetic field (see Fig. 5.5).

If enough energy is supplied, the longitudinal vector can be completely flipped over with a 180-degree clockwise shift in the direction against the external magnetic field. The RF energy pulse required to flip the net longitudinal magnetization vector over is called the “180-degree pulse” (see Fig. 5.6).

The RF energy is provided by an RF electromagnetic coil that transmits an oscillating RF wave at the Larmor frequency to cause nuclear excitation. After the RF pulse is turned off, the excited nuclei go through a relaxation phase. Under the nuclear relaxation phase, the net longitudinal magnetization vector returns to its original state in the thermal equilibrium and the net transverse magnetization vector disappears due to dephasing of the nuclei.

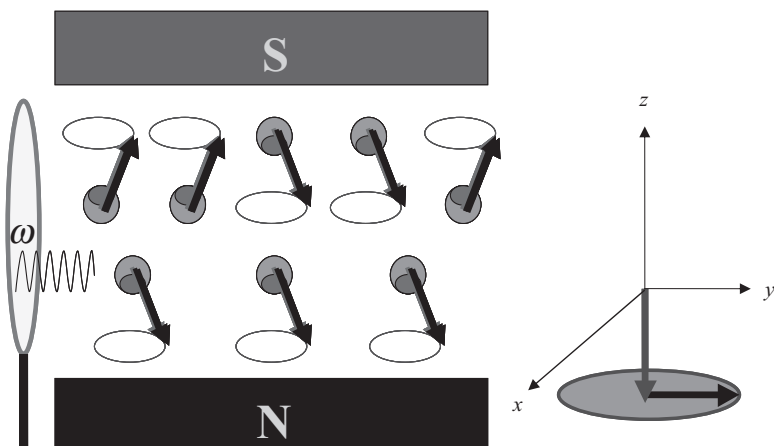


Figure 5.6 The 180-degree pulse causing nuclei to precess in phase with the longitudinal vector shifted clockwise by 180 degrees as a result of the absorption of RF energy at the Larmor frequency.

The energy emitted during the relaxation process induces an electrical signal in an RF coil tuned at the Larmor frequency. The free induction decay of the electromagnetic signal in the RF coil is the basic signal that is used to create MR images. Thus, under the NMR phenomenon, the RF energy received by the nuclei at the Larmor frequency causes characteristic excitation of nuclei. The nuclear excitation forces the net longitudinal and transverse magnetization vectors to move. The movement of longitudinal and transverse vectors can be explained through Bloch's equation as described below (Eq. 5.12) (1–5).

Assuming N to be the total number of spinning nuclei in the object being imaged, a stationary magnetization vector, \vec{M} , can be defined from the available magnetic moments as

$$\vec{M} = \sum_{n=1}^N \vec{\mu}_n. \quad (5.5)$$

Let us now define a rotating frame as a coordinate system with a transverse plane rotating at the angular frequency, ω . Let us define a stationary magnetization vector as \vec{M} with its components in the unit direction vectors \vec{i} , \vec{j} , and \vec{k} respectively, in the direction of the actual coordinate system, x , y , and z , that is also called the laboratory coordinate system. For a rotating frame, let us define the rotating magnetization vector \vec{M}_r with the unit direction vectors \vec{i}' , \vec{j}' , and \vec{k}' , respectively, in the x , y , and z coordinate system as (3, 5, 6)

$$\vec{M} = M_x \vec{i} + M_y \vec{j} + M_z \vec{k}$$

and

$$\vec{M}_r = M_x \vec{i}' + M_y \vec{j}' + M_z \vec{k}'. \quad (5.6)$$

From the rotation transformation (given in Chapter 2), the stationary and clockwise rotating frames are related as

$$\begin{aligned}\vec{i}' &= \cos(\omega t)\vec{i} - \sin(\omega t)\vec{j} \\ \vec{j}' &= \sin(\omega t)\vec{i} + \cos(\omega t)\vec{j} \\ \vec{k}' &= \vec{k}.\end{aligned}\quad (5.7)$$

Thus, the magnetization vectors corresponding to the stationary (laboratory) and clockwise rotating frames can be written as

$$\begin{bmatrix} M_{x'} \\ M_{y'} \\ M_{z'} \end{bmatrix} = \begin{bmatrix} \cos\omega t & -\sin\omega t & 0 \\ \sin\omega t & \cos\omega t & 0 \\ 0 & 0 & 1 \end{bmatrix} \begin{bmatrix} M_x \\ M_y \\ M_z \end{bmatrix}. \quad (5.8)$$

The transverse magnetization vector in the rotating frame can be written as

$$M_{x',y'} = M_{x,y} e^{i\omega t}$$

where

$$M_{x,y} = M_x + iM_y \quad \text{and} \quad M_{x',y'} = M_{x'} + iM_{y'}. \quad (5.9)$$

Let us assume that H_{1r} and H_1 are, respectively, the RF field in the rotating frame and the stationary coordinate systems. Similar to Equation 5.7, an oscillating RF field causing nuclear excitation can be expressed as

$$H_{1r}(t) = H_1(t) e^{i\omega t}$$

with

$$H_1 = H_{1,x} + iH_{1,y} \quad \text{and} \quad H_{1r} = H_{1,x'} + iH_{1,y'}. \quad (5.10)$$

It is to be noted that H_1 is a short-term field produced by the oscillating RF pulse that is much weaker (of the order of a few tens of millitesla). It is turned on only for a few microseconds to milliseconds of nuclear excitation. The external magnetic field, H_0 , is static in nature and much stronger (usually in the range of 0.5–1.5T).

The relationship between the rates of change of stationary magnetization vector \vec{M} and rotating magnetization vector \vec{M}_r can then be expressed as (5)

$$\frac{d\vec{M}}{dt} = \frac{\partial \vec{M}_r}{\partial t} + \omega \times \vec{M}_r. \quad (5.11)$$

From the above formulation, it can be shown that during the RF pulse (nuclear excitation phase), the rate of change in the net stationary magnetization vector can be expressed as (Bloch's equation):

$$\frac{d\vec{M}}{dt} = \gamma \vec{M} \times \vec{H} \quad (5.12)$$

where \vec{H} is the net effective magnetic field.

Considering the total response of the spin system in the presence of an external magnetic field along with the RF pulse for nuclear excitation, followed by the nuclear relaxation phase, the change of the net magnetization vector can be expressed as (3)

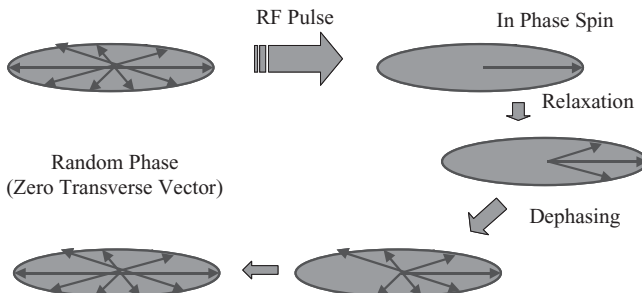


Figure 5.7 The transverse relaxation process of spinning nuclei.

$$\frac{d\vec{M}}{dt} = \gamma \vec{M} \times \vec{H} - \frac{M_x \vec{i} + M_y \vec{j}}{T_2} - \frac{(M_z - M_z^0) \vec{k}}{T_1} \quad (5.13)$$

where \vec{M}_z^0 is the net magnetization vector in thermal equilibrium in the presence of an external magnetic field H_0 only, and T_1 and T_2 are, respectively, the longitudinal (spin–lattice) and transverse (spin–spin) relaxation times in the nuclear relaxation phase when excited nuclei return to their thermal equilibrium state. In other words, the longitudinal relaxation time, T_1 , represents the return of the net magnetization vector in z -direction to its thermal equilibrium state, while the transverse relaxation time, T_2 , represents the loss of coherence or dephasing of spin leading to the net zero vector in the x - y plane. Figure 5.7 shows the transverse relaxation process through spin dephasing.

The solution to above Bloch equations for the transverse and longitudinal magnetization vectors can be obtained through relaxation processes while the system recovers to its thermal equilibrium state. The transverse magnetization equation solution is obtained through a clockwise precession-based spin–spin relaxation process with a decay rate of $1/T_2$ until $\vec{M}_{x,y}(t) \rightarrow 0$. The longitudinal magnetization vector $\vec{M}_z(t)$ decays with a rate of $1/T_1$ through the spin–lattice relation process until it returns to the net magnetization vector in thermal equilibrium, \vec{M}_z^0 . The longitudinal and transverse magnetization vectors with respect to the relaxation times in the actual stationary coordinate system can be given by

$$\begin{aligned} \vec{M}_z(t) &= \vec{M}_z^0(1 - e^{-t/T_1}) + \vec{M}_z(0)e^{-t/T_1} \\ \vec{M}_{x,y}(t) &= \vec{M}_{x,y}(0)e^{-t/T_2}e^{-i\omega_0 t} \\ \text{with } \vec{M}_{x,y}(0) &= \vec{M}_{x,y}'(0)e^{-i\omega_0 t_p} \end{aligned} \quad (5.14)$$

where $\vec{M}_{x,y}(0)$ represents the initial transverse magnetization vector with the time set to zero at the end of the RF pulse of duration τ_p .

Equation 5.14 describes the nature of the change in the transverse and longitudinal magnetization vectors with respect to time after the RF pulse. The exponential decay of e^{-t/T_2} can be seen in the transverse magnetization relaxation shown in Figure 5.8a while the recovery of longitudinal magnetization vector after 90-degree and 180-degree pulses are shown, respectively, in Figure 5.8b,c.

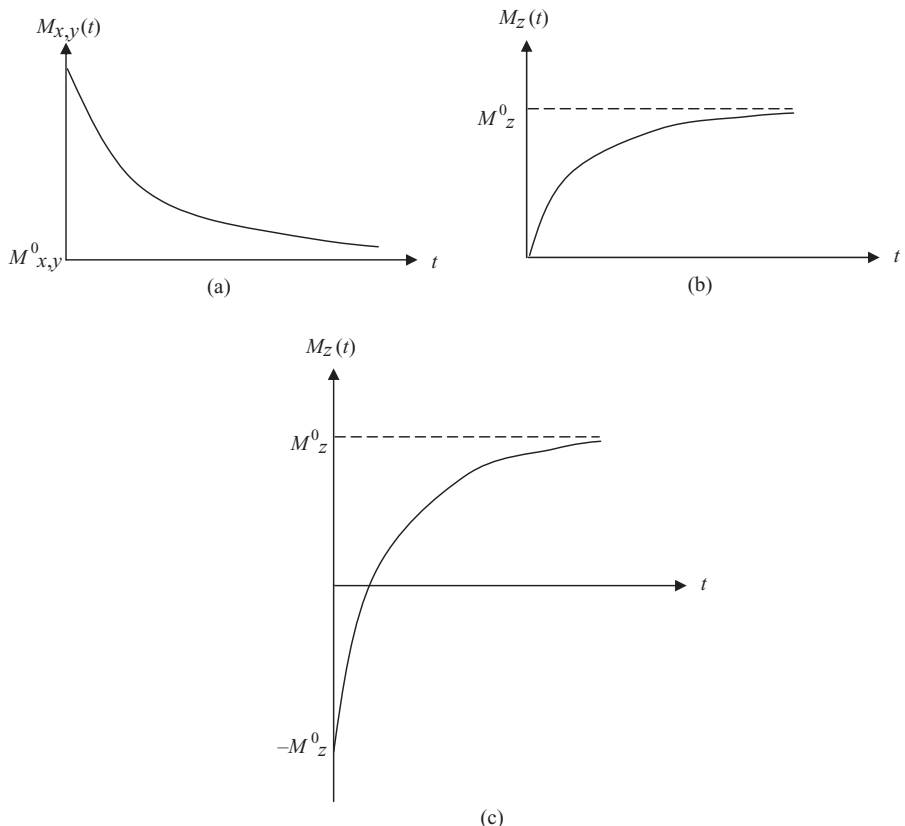


Figure 5.8 (a) Transverse relaxation and recovery to zero transverse magnetization vector after an RF pulse, (b) longitudinal magnetization relaxation and recovery to M_z^0 after the 90-degree RF pulse, and (c) longitudinal magnetization relaxation and recovery to M_z^0 after the 90-degree RF pulse.

As described above, the RF pulse, transmitted through an RF coil, causes nuclear excitation, changing the longitudinal and transverse magnetization vectors. After the RF pulse is turned off, the excited nuclei go through the relaxation phase, emitting the absorbed energy at the same Larmor frequency that can be detected as an electrical signal, called the free induction decay (FID). The FID is the raw NMR signal that can be acquired through the same RF coil tuned at the Larmor frequency.

Let us represent a spatial location vector \mathbf{r} in the spinning nuclei system with a net magnetic field vector $\vec{H}_r(\mathbf{r})$ and the corresponding net magnetization vector $\vec{M}(\mathbf{r}, t)$. The magnetic flux $\phi(t)$ through the RF coil can be given as (5)

$$\phi(t) = \int_{\text{object}} \vec{H}_r(\mathbf{r}) \cdot \vec{M}(\mathbf{r}, t) d\mathbf{r} \quad (5.15)$$

where $\mathbf{r} = x\vec{i} + y\vec{j} + z\vec{k}$.

The voltage induced in the RF coil, $V(t)$, is the raw NMR signal and can be expressed (using Faraday's law) as

$$V(t) = -\frac{\partial \phi(t)}{\partial t} = -\frac{\partial}{\partial t} \int_{object} \vec{H}_r(\mathbf{r}) \cdot \vec{M}(\mathbf{r}, t) d\mathbf{r}. \quad (5.16)$$

The realization of a spatial location-dependent signal in Equation 5.16 is important to create an MR image that maps the MR response of the spinning nuclei available in that location. Since the Larmor or precession frequency is based on the net magnetic field, if an additional magnetic gradient field is superimposed on the static external magnetic field, the spatial locations within the object can be encoded with localized specific precession frequencies. Thus, spatial locations within the object that is placed inside a large magnet (producing the static external magnetic field) can be viewed as small volumes containing nuclei that can be excited using different RF frequencies. NMR signals generated by specific excited volumes within the object can thus be differentiated with respect to the individual RF frequencies. Access to the small volumes within the object to generate corresponding NMR signals is obtained through spatial encoding techniques. These techniques utilize different gradient methods for frequency- and phase-based spatial encoding. Once the spatial locations with an object being imaged are accessed, the corresponding NMR signals are acquired using specific RF pulse sequences for image reconstruction. NMR signals are mapped into the image of the object with the spatial relationship between the object and image spaces. An image reconstruction process assigns values to the image pixels (in case of two-dimensional [2-D] images) or voxels (in case of three-dimensional [3-D] images) displaying a particular feature associated with the NMR phenomenon of the nuclei present in the corresponding volume. The application of a specific pulse sequence determines the feature associated with the specific image pixels or voxels. The conventional MR images take advantage of three common parameters of nuclei: spin density (density of nuclei), longitudinal relaxation time T_1 , and transverse relaxation time T_2 . Several versions of the image with different weightings of the NMR parameters (spin density, T_1 , and T_2) can be reconstructed using computer processing and reconstruction methods in association with selected pulse sequences.

Since the NMR signal is collected in the frequency domain, the spatial information of the image can be obtained by taking a Fourier transform with appropriate dimensions. More details on image reconstruction methods for MRI are described in Chapter 8. The basic form of MRI can be described using the 3-D Fourier transform-based reconstruction method. This method is also called the FID method in which the spin echoes are formed using RF pulse sequences for 3-D spatial location (volume) selection. Let us assume that three gradient fields, G_x , G_y , and G_z , are, respectively, applied in x -, y -, and z -directions for the selection and excitation of a spatial location (volume) with a spin nuclei density $\rho(x, y, z)$. The overall gradient $\mathbf{G}(t)$ for a spatial location, \mathbf{r} , is expressed as

$$\mathbf{G}(t) = G_x(t)\vec{i} + G_y(t)\vec{j} + G_z(t)\vec{k}. \quad (5.17)$$

From Equation 5.14, after some simplifications and assumptions such as field homogeneity and absence of chemical shifts, the NMR spin-echo signal, $S(t)$, from a specific location or volume of the object can be expressed as

TABLE 5.1 Typical T_1 and T_2 Relaxation Times and the Spin Density (SD) of Some of the Tissues and Fluids Present in the Human Body

Tissue	T_1 (ms)	T_2 (ms)	SD (%)
Fat	150	150	10.9
Liver	250	44	10.0
White matter	300	133	11.0
Gray matter	475	118	10.5
Blood	525	261	10.0
CSF	2000	250	10.8

$$S(t) = \int \vec{M}(\mathbf{r}, t) d^3r \quad (5.18)$$

where $\vec{M}(\mathbf{r}, t) = \vec{M}_0 \rho(\mathbf{r}) e^{-i\gamma\mathbf{r} \cdot \int_0^t \mathbf{G}(t') dt'}$ and \vec{M}_0 is the magnetization vector in thermal equilibrium.

Let ω_x , ω_y , and ω_z be the angular frequencies corresponding to the gradient fields, G_x , G_y , and G_z , respectively, Equation 5.18 can be further simplified as (3):

$$\rho(\omega_x, \omega_y, \omega_z) = \vec{M}_0 \iiint \rho(x, y, z) e^{-i(\omega_x x + \omega_y y + \omega_z z)} dx dy dz. \quad (5.19)$$

The MR image of the spin density can then be reconstructed from the FID signal, $S(t)$, by taking a 3-D inverse Fourier transform (from frequency domain to the spatial domain) as (3)

$$\rho(x, y, z) = \vec{M}_0 \iiint S(\omega_x, \omega_y, \omega_z) e^{i(\omega_x x + \omega_y y + \omega_z z)} d\omega_x d\omega_y d\omega_z. \quad (5.20)$$

Table 5.1 shows typical T_1 and T_2 relaxation times and the spin density of some of the tissues and fluids present in the human body. It can be seen that there is considerable change in relaxation parameters of tissues and fluids of interest such as blood and cerebrospinal fluid (CSF). Once NMR raw signals are acquired and MR parameters are computed, the contrast in an image can be adjusted by changing the respective weights of the parameters. Normally the spin-density images are weighted by the T_1 parameter to improve contrast features of anatomical structures.

5.2. MR INSTRUMENTATION

The stationary external magnetic field for MRI of the human body is provided by a large superconducting magnet with a typical strength of 0.5 to 1.5 T. The magnet is required to have a 30–50 cm diameter spherical volume for the human body and housing of gradient coils as needed. A diagnostic-quality imaging system requires a magnet with good field homogeneity, typically on the order of 10–50 ppm. For high-quality spectroscopy and fMRI, a set of shim coils is used to provide an addi-

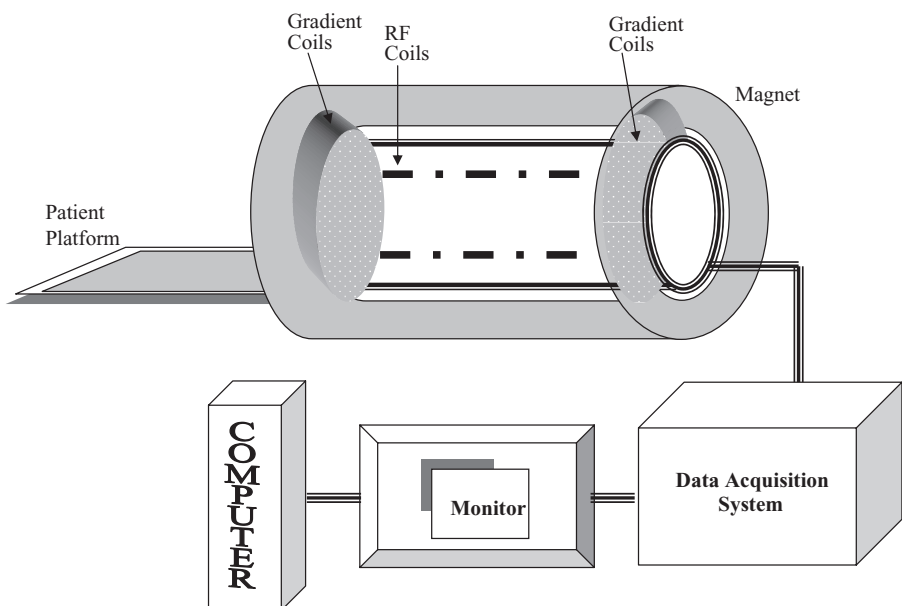


Figure 5.9 A general schematic diagram of an MRI system.

tional magnetic field to compensate for the field inhomogeneity of the main magnet. A general schematic of an MRI system is shown in Figure 5.9.

In typical MRI systems, three orthogonal gradient coils are used to provide gradient magnetic fields (1, 3). Although the gradient coils generate magnetic fields in the z -direction, they provide software-controlled displacements in the x -, y -, and z -directions. The simplest form of gradient coil generates a linear, spatially dependent magnetic field. Field strength, linearity, and switching time are three important considerations for the selection of gradient coils. The shape and placement of the coil are crucial for generating the field in the desired direction. The Golay-type coils are commonly used for x - and y -direction gradients, while a double loop-based Helmholtz coil is typically used for the z -direction gradient.

During the nuclear excitation phase, an RF coil with electronic circuitry is used to transmit time-varying RF pulses. The same RF coil with computerized programming and switching control is used to receive the RF emissions during the nuclear relaxation phase. The NMR signal, as described above, is recorded through FID in the RF coil at a selected RF. The computerized control of electronic circuitry allows the programming of the RF coil to transmit and receive specific RF pulses as required by the pulse sequences for image reconstruction. The RF transmitter section includes a wave synthesizer, RF modulator, RF amplifier, and a coupler that couples the RF signal to the RF coil. The RF receiver section uses the coupler to switch the signal from the RF coil to an assembly of pre-amplifiers and demodulators. The FID signal thus received is then sent to an analog-to-digital converter to record the data in digital format.

5.3. MRI PULSE SEQUENCES

To obtain MR images, a spatial encoding has to be established between the object and image coordinate systems. As described above, the spatially encoded locations or volumes are first excited through RF pulses and then accessed to acquire the FID signal during the relaxation phase for image reconstruction. Various sequences of RF pulses for spatial encoding and signal acquisition have been designed for MRI. These sequences are based on different methods that can be exploited to improve the SNR and scanning rate of a 3-D object. To understand the design of RF pulse sequences let us first understand the process of spatial encoding and the coordinate system. Figure 5.10a shows a 3-D object with an x - y - z object coordinate system that can be scanned to provide three different orientations of image views: axial, sagittal, and coronal. Figure 5.10b shows axial, sagittal, and coronal images of a human brain. Usually, a patient is oriented on the platform shown in Figure 5.9 for axial imaging with the spine aligned in the z -direction (1–5).

The encoding of the NMR signal has to be performed in all three dimensions to scan the object and reconstruct its 3-D images. This means that all three dimensions have to be encoded with spatially dependent coding of NMR signals. As with any other RF wave, the NMR signal has two basic features: the frequency and the phase. For this reason, there are two basic methods of spatial encoding in MRI: frequency encoding and phase encoding.

In frequency encoding, a linear gradient is applied throughout the imaging space along a selected direction (such as the z -direction). As described above, the precession or Larmor frequency is dependent on the net magnetic field at the location of the spinning nuclei. If a linear gradient is superimposed on the stationary magnetic field of the external magnet, the net magnetic field is spatially encoded along the direction of the gradient and consequently the effective Larmor frequency of spinning nuclei is also spatially encoded along the direction of the gradient as shown in Figure 5.11. Thus, a linear gradient can be used along the z -direction for slice selection for axial imaging.

After the slice selection through frequency encoding using a linear gradient along the z -direction, x - and y -directions need to be spatially encoded for 3-D imaging. This is accomplished by further encoding the phase of the spinning nuclei along the x -direction of the selected slice while the spatial encoding in the y -direction is provided by another linear frequency encoding gradient along the y -direction. In such a scanning method, a linear frequency encoding gradient along the y -direction is also used for reading out the NMR signal. This is further explained below for spin-echo pulse sequences.

The phase-encoding gradient is applied as a constant step gradient in the direction in which all of the spinning nuclei are spinning with the same Larmor frequency. A fixed magnitude of the gradient changes the phase of the spinning nuclei by a respective fixed amount. Since the spatial encoding in two directions is provided by linear frequency encoding gradients, a step function-based gradient field can be applied in the third direction for phase encoding to acquire NMR signals for 3-D scanning and imaging. Unlike frequency encoding, the phase-encoding gradient is applied in steps with repeated cycles. For example, if 256 steps are to be applied in

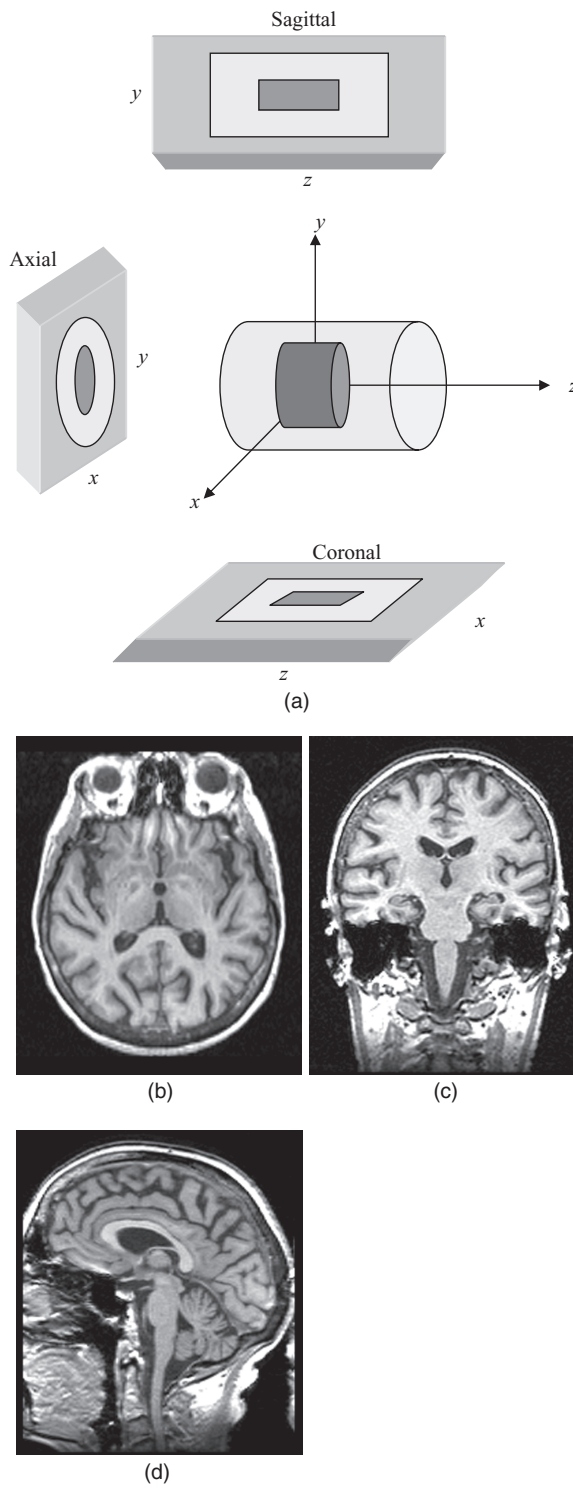


Figure 5.10 (a) Three-dimensional object coordinate system with axial, sagittal, and coronal image views. (b) From top left to bottom right: Axial, coronal, and sagittal MR images of a human brain.

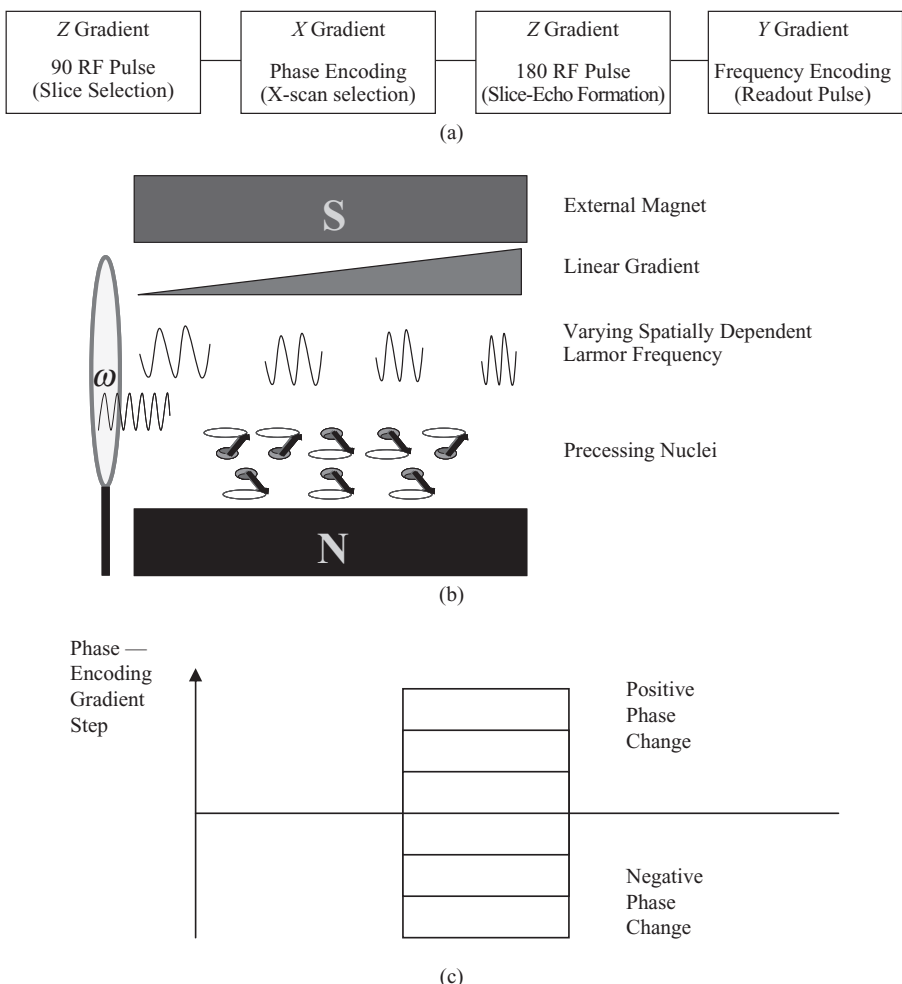


Figure 5.11 (a) Three-dimensional spatial encoding for spin-echo MR pulse sequence. (b) A linear gradient field for frequency encoding. (c) A step function-based gradient field for phase encoding.

the phase-encoding gradient, the readout cycle is repeated 256 times, each time with a specific amount of phase-encoding gradient.

5.3.1 Spin-Echo Imaging

Let us understand the formation of a spin echo, a commonly used method in NMR imaging. If an axial image of the human brain is to be reconstructed, an axial slice of the brain in the object coordinate system is selected by applying a linear frequency encoding gradient in the z -direction. Along with the gradient, a 90-degree pulse can be applied to cause nuclear excitation in the entire slice volume. During the time a

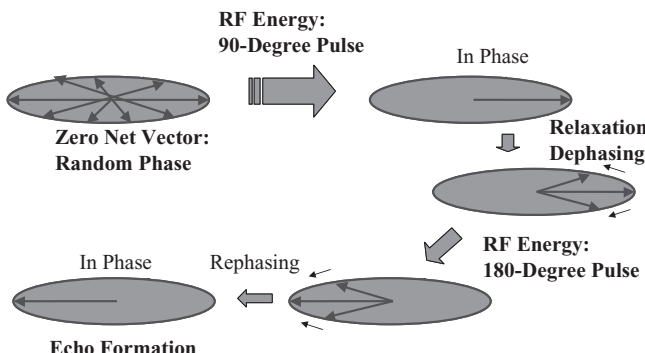


Figure 5.12 The transverse relaxation and echo formation of the spin-echo MR pulse sequence.

frequency encoding gradient is established and applied for slice selection along the z -direction, a phase shift is introduced in the selected volume. To avoid any loss of signal due to dephasing and phase shift, a rephasing gradient pulse is usually applied, as shown in Figure 5.12. To obtain a 2-D image of the selected slice, spatial encoding gradients are applied in the x - and y -directions. A phase-encoding gradient is applied in the x -direction after the 90-degree pulse has been applied for nuclear excitation in the slice volume. The 90-degree pulse causes the spinning nuclei to precess in phase. After the 90-degree pulse, the spinning nuclei start dephasing in the transverse direction while the net longitudinal magnetization vector starts returning to the state of thermal equilibrium. As shown in Figure 5.12, if a 180-degree pulse is applied along the z -direction before the spinning nuclei lose their coherence, the transverse magnetization vector is flipped in the reverse direction and the spinning nuclei start rephasing themselves to produce an echo exactly after the time lag between the 90-degree and 180-degree pulses. Thus, the time for echo formation, T_E , is defined between the application of the 90-degree pulse and the formation of echo (rephasing of nuclei). The time between the 90-degree pulse and 180-degree pulse is $T_E/2$, which is the same as the time between the 180-degree pulse and the formation of echo. At the formation of spin echo, the NMR signal is read through the readout frequency encoding gradient (along the y -direction). It should be noted that to implement a phase-encoding gradient with N steps, the readout cycle is repeated N times to collect phase-encoded echoes from different locations along the x -direction.

The frequency-encoded spin echoes can be mapped into a raw data space, called a “ k -space.” The k -space represents the placement of raw frequency data collected through the pulse sequences in a multidimensional space in which an image is to be reconstructed. The transformation from the frequency signal-based k -space to the image space is one of the most commonly used methods for MR image reconstruction. Thus, by taking the inverse Fourier transform of the k -space data, an image of the object can be reconstructed in the spatial domain. For example, a 2-D k -space can be used to map the raw spin-echo data for a selected slice along the z -direction. This k -space then represents the echo signals that are encoded with frequency and

phase along the respective x - y directions. The NMR signals collected as frequency-encoded echoes can be placed as horizontal lines in the corresponding 2-D k -space. As multiple frequency encoded echoes are collected with different phase-encoding gradients, they are placed as horizontal lines in the corresponding k -space with the vertical direction representing the phase-encoding gradient values. After all spin echoes are collected, the k -space is complete with the raw frequency data. A 2-D inverse Fourier transform of the k -space data can provide a 2-D MR image of the selected slice.

It is clear from the above discussion that spin-echo pulse sequences are repeatedly applied to scan the entire object or, in other words, to complete the k -space frequency information. Before the next pulse sequence for echo formation and signal readout is started, the spinning nuclei are provided some time for longitudinal and transverse relaxations, bringing them close to the thermal equilibrium. The time period between the applications of two consecutive spin-echo pulse sequences is called the cycle repetition time, T_R . The manipulation of T_E and T_R times provides different weighting of T_1 and T_2 relaxation times as the longitudinal and transverse relaxation processes are directly affected by the selection of echo formation and cycle repetition times. It can be seen from Figures 5.12 and 5.13, if the time between the 90-degree pulse and 180-degree pulse is long, the spinning nuclei would almost lose their coherence depending on the T_2 relaxation time. Thus, the NMR signal at

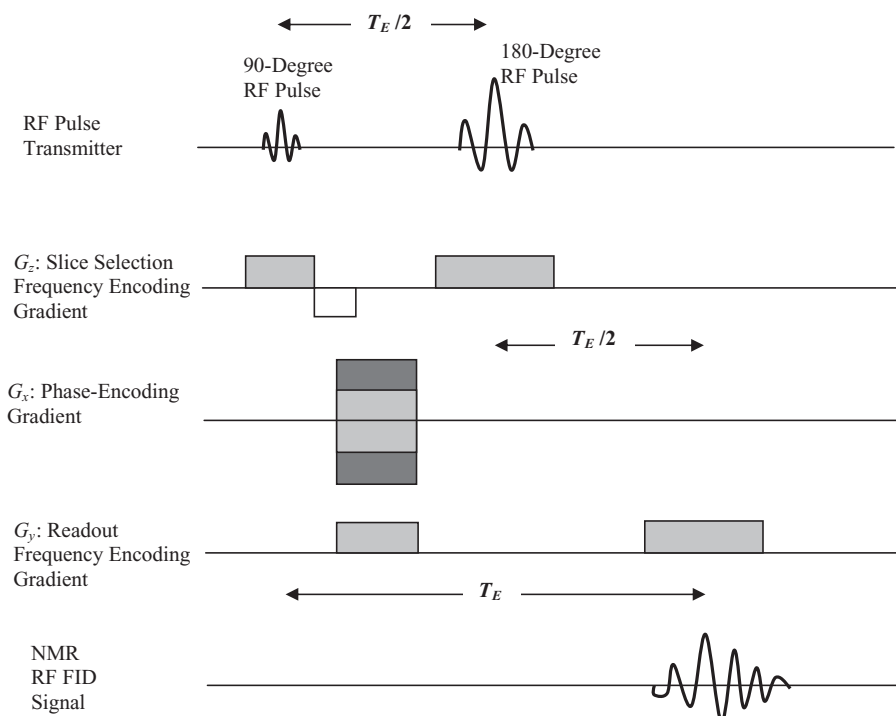


Figure 5.13 A spin-echo pulse sequence for MRI.

the formation of the echo would be largely influenced by the T_2 relaxation time if the 90-degree pulse was applied when the spinning nuclei were in (or were close to) thermal equilibrium. This means that T_2 -weighted MRI requires a long T_R and a long T_E -based spin-echo pulse sequence. On the other hand, a short T_R and a short T_E -based spin-echo pulse sequence would provide T_1 -weighted MRI. In this case, a short T_R would not allow the spinning nuclei to complete longitudinal relaxation, leaving the NMR signal at the short-time-based echo formation with T_1 influence. From these concepts, it can be easily understood that a long T_R - and a short T_E -based spin-echo pulse sequence would provide neither T_1 - nor T_2 -weighted MRI. As a matter of fact, in the absence of T_1 and T_2 influences, the long T_R and short T_E -based spin-echo pulse sequences provide spin-density (also called proton density) MR images. A short T_R - and a long T_E -based spin-echo pulse sequence are not used for MRI for obvious reasons. Equations 5.13 and 5.14, as described earlier in this section, present the mathematical representation of the dependency of longitudinal and transverse magnetization vectors on T_1 and T_2 relaxation times. Following Equations 5.13–5.19, the relationship of echo signal intensity and T_1 and T_2 relaxation times can be expressed as

$$\rho(x, y, z) = \rho_0(x, y, z) \left\{ e^{-\frac{T_E}{T_2}} \right\} \left\{ 1 - e^{-\frac{T_R}{T_1}} \right\} \quad (5.21)$$

where $\rho_0(x, y, z)$ is the initial spin density function.

The exponential decay terms of T_E/T_2 and T_R/T_1 in Equation 5.21 confirms that a short T_R and short T_E would lead to T_1 -weighted imaging, while long T_R and long T_E would provide T_2 -weighted imaging. As can be seen in Figure 5.1, T_1 -weighted, T_2 -weighted, and spin-density MR images of the same slice provide different tissue contrast in the respective images. This is a very useful feature in diagnostic radiology for lesion detection and characterization.

There are several factors that affect the MR signal acquisition, causing artifacts or degradation in the reconstructed image. These factors include field inhomogeneities, flow of nuclei, and change in resonance parameters due to chemical shifts within the object. Magnetic field inhomogeneities and gradient fields cause a direct dephasing effect to the transverse relaxation process. The effective transverse relaxation time, T_2^* from the field inhomogeneities can be expressed as

$$\frac{1}{T_2^*} = \frac{1}{T_2} + \frac{\gamma \Delta H}{2} \quad (5.22)$$

where ΔH is the field inhomogeneities representing the maximum deviation of the field strength over the imaging volume. When a spatial encoding gradient is applied along any direction to localize the distribution of nuclei, the transverse relaxation time is further reduced to T_2^{**} and can be expressed as

$$\frac{1}{T_2^{**}} = \frac{1}{T_2^*} + \frac{\gamma Gd}{2} \quad (5.23)$$

where G is the strength of the gradient field applied over the region of diameter d .

Magnetic susceptibility caused by the presence of other substances in the imaging medium is another important factor influencing relaxation times. For

example, blood products such as deoxyhemoglobin, intracellular methemoglobin, ferritin, and other substances such as calcium present in the human body can cause inhomogeneities in the local magnetic field. Also as a result of the diffusion of protons within the tissue, the local magnetic fields are altered within the imaging volume. The loss in signal due to magnetic susceptibility can cause artifacts in the T_2 -weighted and spin-density images. These effects could be significant in blood flow imaging.

The complex effects caused by the flow of protons and other substances in and out of the imaging volumes due to diffusion, perfusion, and blood flow could be turned around to allow visualization of moving protons leading to useful imaging methods such as MR perfusion imaging and MR angiography (3–5). A random diffusion of protons causes a loss of signal due to phase cancellation in the dephasing mechanism. Thus, useful information about water proton diffusion and its direction can be observed through appropriate MR pulse sequences. In MRI, the diffusion is defined as a random motion of water protons with a slower motion on the order of a few microns per millisecond. Perfusion is described by one of three mechanisms. A perfusion can involve the transition of a nondiffusible contrast agent through the microvasculature, or it can be described as the fast flow of water protons into a selected imaging volume. These perfusion processes can define the physiological behavior of a tissue or lesion and can be detected through the relaxation time parameters. However, perfusion can be forced into a tissue through a diffusible tracer in the extravascular space. The performance of perfusion imaging depends on the contrast agent (such as fluorine) and usually provides a low SNR. Volume averaging becomes necessary to improve the SNR for better image quality that limits the image resolution. However, the use of a perfusion contrast agent can provide important information about changes in the tissue behavior in the early stages of many critical brain diseases.

Another important factor that causes alterations in relaxation times is the presence of a molecular or chemical environment that can change the characteristic magnetic influence on the protons. This effect, called chemical shift, can cause minor deviations in the Larmor frequency of spinning protons depending on their molecular environment. For example, water protons present in fat will precess at a slightly different frequency than the protons in water. To minimize artifacts caused by the chemical shift phenomenon, larger bandwidth frequency encoding is done in MR pulse sequences with short echo times.

5.3.2 Inversion Recovery Imaging

As described above, MR FID signal can be generated in the relaxation (also called inversion recovery [IR]) process after applying the 180-degree pulse. Spin-echo imaging sequence as described in Figure 5.13 can also be applied in the inversion recovery process. In spin-echo imaging sequence, a slice is selected through frequency encoding gradient with a 90-degree pulse that creates a spin-lattice magnetization with all protons in the selected slice. IR imaging pulse sequence allows relaxation of some or all of T_1 before spins are rephased through 90-degree pulse and therefore emphasizes the effect of longitudinal magnetization. In IR imaging pulse sequence, 180-degree pulse is first applied along with the slice selection

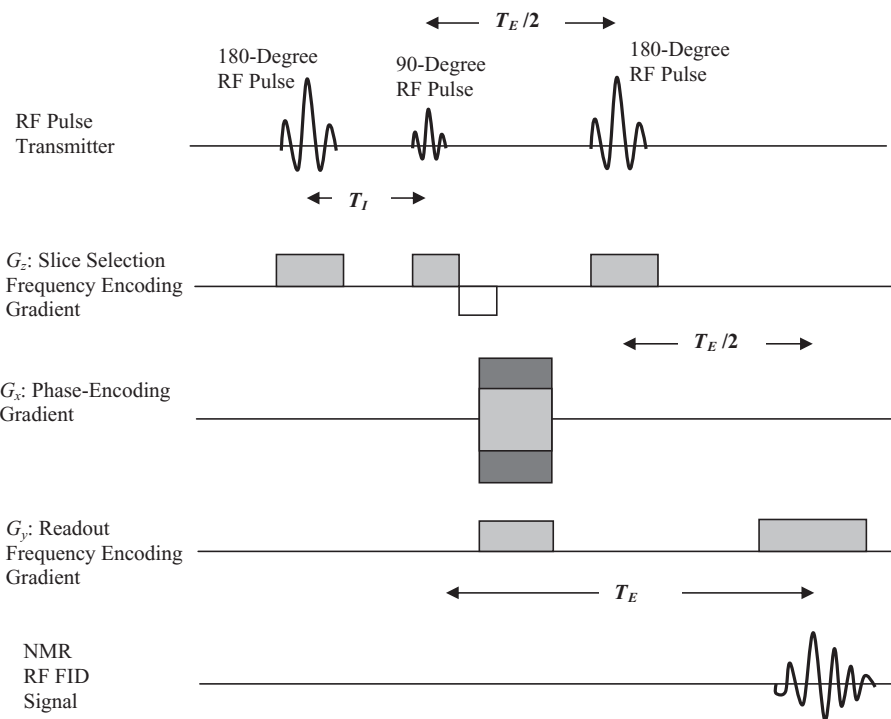


Figure 5.14 Inversion recovery (IR) pulse sequence for MR imaging.

frequency encoding gradient as shown in Figure 5.14. After the time T_1 equivalent to the recovery of T_1 time ($T_1 = T_1 \ln 2$), a 90-degree pulse is applied to start the spin-echo imaging pulse sequence. The rest of the imaging sequence is the same as described above in spin-echo imaging as 180-degree pulse is applied after $T_E/2$ time to create an echo. In the mean time, phase-encoding gradient is applied along the x -direction. The readout frequency encoding gradient is applied along the x -direction to record the echo FID (Fig. 5.14). Figure 5.15 shows a coronal image of the brain with IR imaging pulse sequence. The emphasized effect of longitudinal magnetization can be seen in the IR image.

5.3.3 Echo Planar Imaging

Echo planar imaging (EPI) is a fast scanning method for 2-D and 3-D MRI. Multiple echo-based measurements are obtained within one T_R cycle time. Multiple echoes are obtained with a single 90-degree RF selective pulse through an oscillating gradient rather than through application of a 180-degree phase reversal pulse as done in the spin-echo pulse sequences. Figure 5.16 shows the EPI pulse sequence for 2-D MRI. The slice selection is obtained through the frequency encoding gradient along the z -direction along with the 90-degree RF selective pulse. An oscillating gradient along the x -direction causes the phase reversal of the spinning nuclei to create periodic echoes. A small readout gradient is applied along the y -direction. This

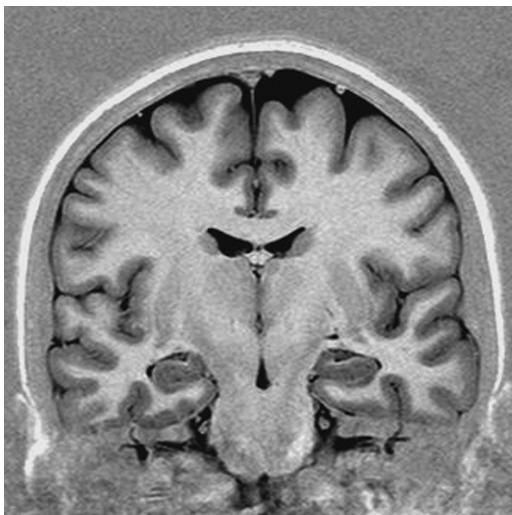


Figure 5.15 A coronal image of human brain obtained through MR inversion recovery imaging pulse sequence.

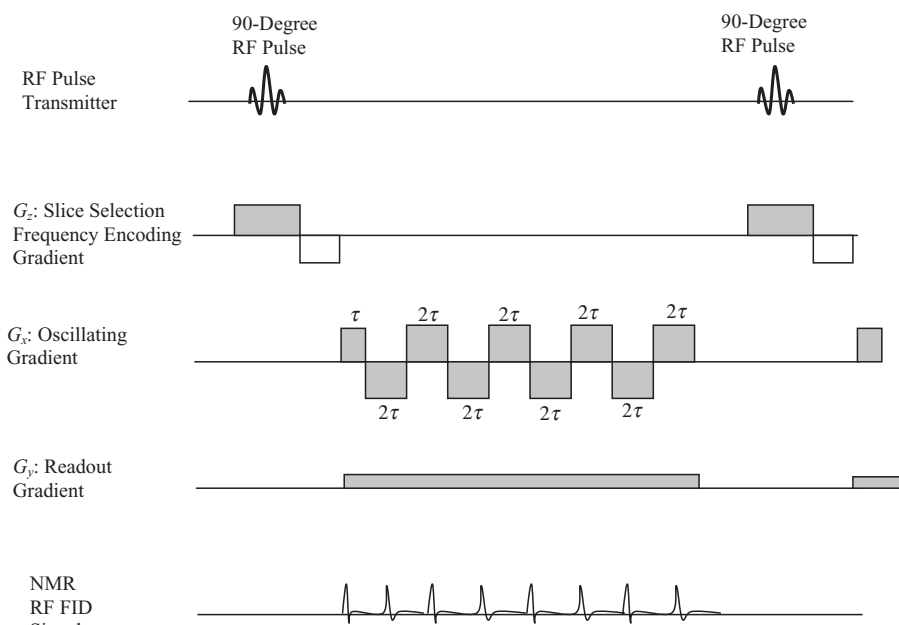


Figure 5.16 A single-shot EPI pulse sequence.

method creates a trajectory in the k -space to provide raw data points. The k -space trajectory of the EPI method as shown in Figure 5.17 creates subsampling of the frequency space. However, the entire image can be obtained in a single shot. Due to the signal decay by the T_2 relaxation time, the number of sampling points in the

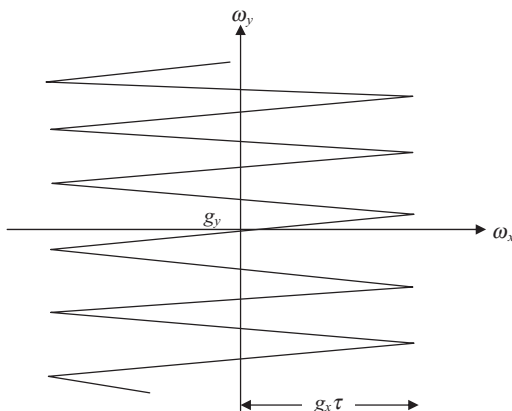


Figure 5.17 The k -space representation of the EPI scan trajectory.

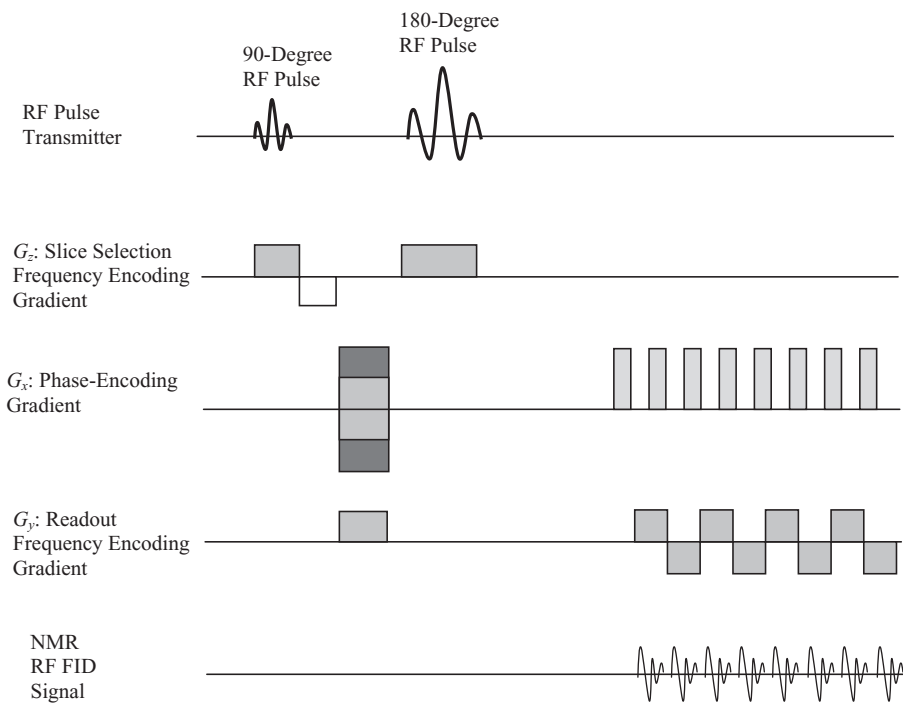


Figure 5.18 An echo planar imaging (EPI) sequence for MR imaging.

k -space is limited. This limitation causes low-resolution images with some degradation. As can be interpreted from k -space representation, the single-shot EPI sequence requires a rapidly oscillating gradient with a large magnitude, which is often difficult to achieve in practice (3, 5).

A variant to single shot EPI pulse sequence shown in Figure 5.18 utilizes the 90- to 180-degree pulse sequence commonly used in spin-echo imaging. After spin

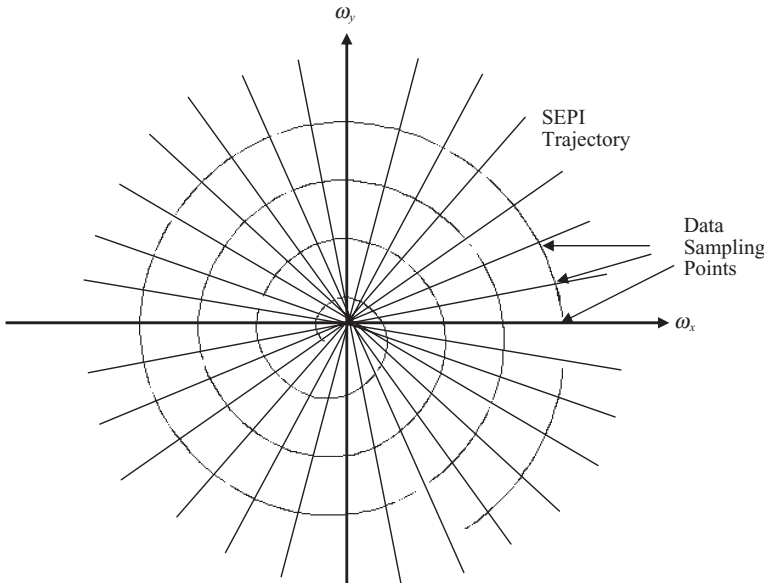


Figure 5.19 The spiral scan trajectory of SEPI pulse sequence in the k -space.

rephasing by 180-degree pulse, this EPI pulse sequence uses periodic phase gradient impulses synchronized with readout frequency encoding gradient impulses to record multiple echoes. A phase-encoding gradient can be placed between 90- and 180-degree pulses to adjust echo time T_E or even can be placed after the 180-degree pulse to minimize T_E .

An alternate approach for fast MRI without the need of a large oscillating gradient is called spiral echo planar imaging (SEPI). In this method, the entire k -space is covered with a spiral scan yielding a circularly symmetric response function that reduces the artifacts in the image. The more uniform distribution of frequency sampling in the k -space can be obtained by the spiral scan as shown in Figure 5.19. It can be shown that for such a spiral scan trajectory in the k -space, the required gradient in the x - and y -directions can be expressed as

$$G_x(t) = \frac{1}{\gamma} \frac{d}{dt} \omega_x(t)$$

$$G_y(t) = \frac{1}{\gamma} \frac{d}{dt} \omega_y(t)$$

where

$$\begin{aligned} \omega_x(t) &= \gamma \lambda t \cos \xi t \\ \omega_y(t) &= \gamma \lambda t \sin \xi t \end{aligned} \quad (5.24)$$

where the spiral scan is obtained through two sin and cosine waves with an angular frequency ξ and amplitude λ .

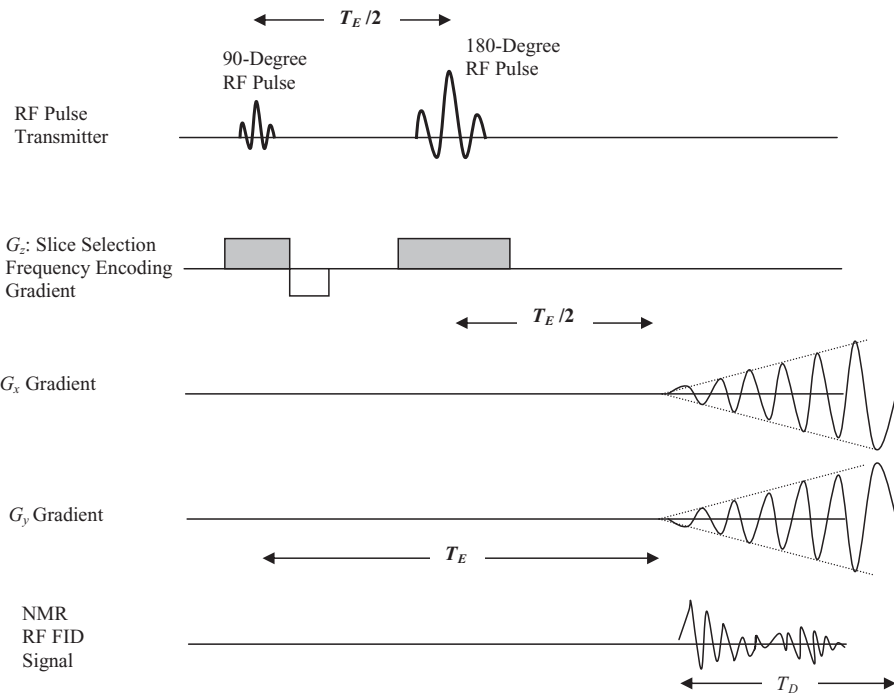


Figure 5.20 A spiral EPI pulse sequence.

In the SEPI pulse sequence (Fig. 5.20), a 90-degree selective RF pulse is applied with the frequency encoding slice selection gradient along the z -direction. This is followed by the 180-degree pulse to prepare the system for the generation of echoes. After the T_E time, that is twice the time duration between the 90-degree and 180-degree RF pulses, a sinusoidal gradient is applied in the x -direction. At the same time, a phase-shifted version or a cosine gradient is applied in the y -direction. The wave gradients in the x - and y -directions cause the required phase reversal for generating the raw data in the k -space with a spiral sampling scan (3, 6). The data are collected through the data collection time, T_D , as shown in Figure 5.20.

Figure 5.21 shows a sequence of 16 brain images obtained through a single-shot SEPI sequence. These slices were obtained in 1.5 s with a resolution of 105×100 pixel and slice thickness of 6 mm. The lower resolution and artifacts can be noticed in these images.

5.3.4 Gradient Echo Imaging

The EPI pulse sequences provide multiple echoes for obtaining NMR signals for image reconstruction through a single shot, that is, a single RF excitation pulse. The collection of data for an entire image through a single excitation pulse has a major disadvantage of yielding low-resolution images because of the T_2 relaxation time decay. Gradient echo imaging methods as applied to a fast low angle shot

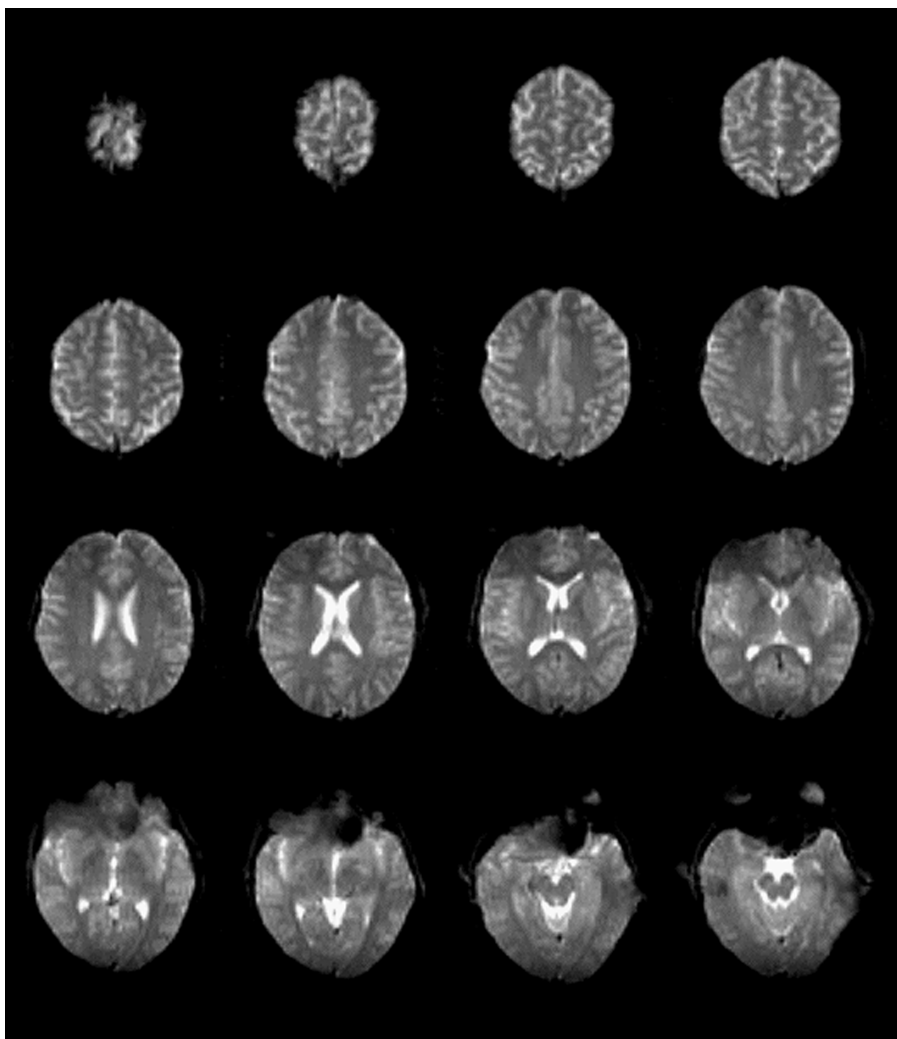


Figure 5.21 MR images of a human brain acquired through SEPI pulse sequence.

(FLASH) imaging sequences utilize low-flip angle RF pulses to create multiple echoes in repeated cycles to collect the data required for image reconstruction (3, 5). Thus, there are more sampling points in the k -space available to reconstruct images at higher resolution. The FLASH pulse sequence, as shown in Figure 5.22, uses a low-flip angle (as low as 20 degrees) RF selective pulse for nuclear excitation. The frequency encoding gradient is applied along the z -direction for slice selection. The slice selection gradient G_z is inverted after the RF pulse to help rephase the spinning nuclei. Since a phase-encoding gradient is applied in the x -direction, the pulse sequence has to be repeated for the number of steps used in phase-encoding. The readout gradient, similar to spin-echo sequence, is applied

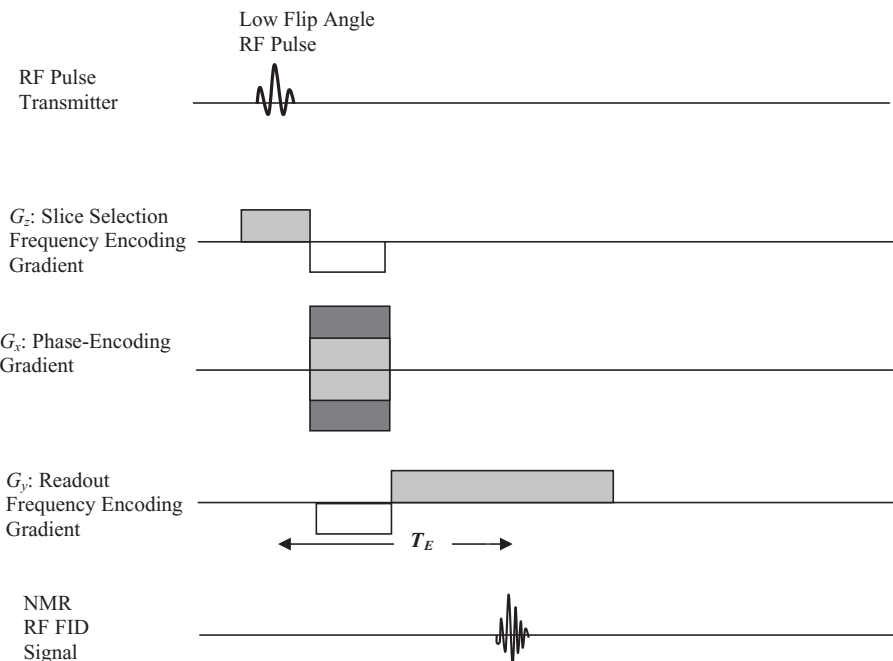


Figure 5.22 The FLASH pulse sequence for fast MR imaging.

along the y -direction. The major difference between spin-echo and gradient echo pulse sequences is that the longitudinal magnetization is not flipped by 90 degrees for nuclear excitation. Instead, a low-flip angle is used to affect the longitudinal magnetization by a small fraction. In addition, there is no 180-degree pulse in the gradient echo cycle, forcing a complete reversal of the spinning nuclei to create an echo. In a FLASH pulse sequence, the readout gradient is inverted to rephase nuclei leading to the gradient echo during the data acquisition period. Since a small flip in the longitudinal magnetization vector is used, the entire pulse sequence time is much shorter than the spin-echo pulse sequence, typically in the range of 10–20 ms.

5.4. FLOW IMAGING

One of the major advantages of MRI is the ability to track flow during image acquisition leading to diffusion (incoherent flow) and perfusion (partially coherent flow) imaging. Equation 5.17 defines the net time-varying gradient at a location vector \mathbf{r} as a vector sum of 3-D gradients (3, 5). There are additional time varying magnetization effects and fields generated by time-varying RF fields, the flow of nuclei being imaged, and other paramagnetic substances. The effect of a bipolar gradient pulse after the 90-degree RF nuclear excitation pulse in generating an FID signal can be split into two parts. The first part is the FID signal generated in the RF receiver coil

by the fixed nuclei and position-independent factors. Such a signal provides a net zero value when it is integrated over a symmetric bipolar gradient pulse without any consideration of relaxation processes. The second part is the FID signal generated in the RF receiver coil by the moving nuclei and velocity-dependent factors. It can be shown that a similar effect is obtained when a unipolar gradient pulse is applied during the 180-degree pulse in the spin-echo sequence. Such a flux, $\phi_v(t)$, can be expressed as (1, 3)

$$\phi_v(t) = \gamma \vartheta \int_0^t G_z(t) t dt \quad (5.25)$$

where τ is the duration of the unipolar gradient pulse and ϑ is the flow velocity.

Figure 5.23 shows a spin-echo sequence for flow imaging. The slice selection gradient, G_z , is applied along the z -direction during the 180-degree phase to provide the flow velocity component in the FID signal. The phase-encoding gradient G_x and readout frequency encoding gradient G_y are similar to the conventional spin-echo pulse sequence. It should be noted that additional gradient pulses need to be incorporated along the x - and y -directions if the flow velocity components in these directions are to be compensated in imaging.

As shown above, the velocity component of spinning nuclei along the direction of the magnetic field gradient induces a proportional phase shift in the transverse

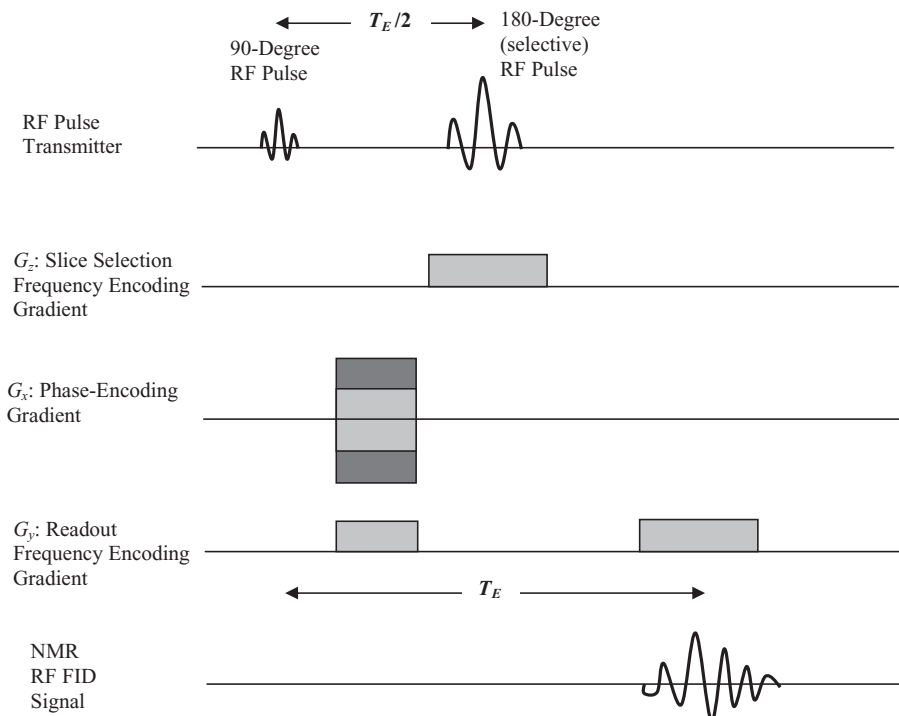


Figure 5.23 A flow imaging pulse sequence with spin echo.

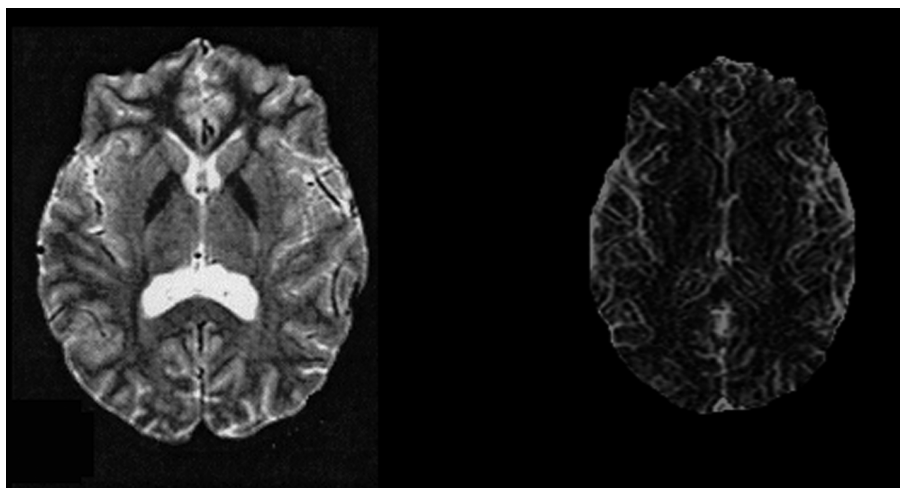


Figure 5.24 Left: A proton density image of a human brain. Right: The corresponding perfusion image.

magnetization. Any change in the velocity component causes dispersion in the phase that leads to unequal signal losses. Thus, phase sensitivity due to the flow is inherent in MR signal generation and is exploited in MRI for conventional flow measurements. Figure 5.24 shows an axial proton density image of a human brain with the corresponding perfusion image showing the vascular structure and flow.

The phase-sensitive methods for conventional flow measurement as described above do not provide accurate imaging and assessment of in-flow. When a specific slice or volume under flow is imaged through repeated pulse sequences, the phase sensitivity causes a loss in the signal but the in-flow of fresh nuclei leads to an increase in the signal intensity at the same time. In in-flow-sensitive or time-of-flight methods, longitudinal magnetization is exploited, making the signal insensitive to flow-induced phase shifts transverse magnetization. The ability to measure specific in-flow in predetermined directions leads to MR angiography. For example, time-of-flight angiography can be performed using a spin-echo imaging sequence where the slice selective 90- and 180-degree pulses have different frequencies. The 90-degree pulse excites protons in one plane while the 180-degree pulse excites protons in another plane. With blood flow, the protons move from a 90-degree plane to a 180-degree plane because of flow, they are rephased and an echo is formed. If there is no blood flow, the protons in the 180-degree plane will not go through echo formation. Contrast-enhanced angiography is performed using a paramagnetic contrast agent that is injected in the blood. The contrast agent reduces spin-lattice relation time T_1 in blood vessels. MR contrast-enhanced angiography uses fast volume imaging pulse sequences with a short TR. There have been a number of recent developments in 3-D MR volume angiography utilizing fast gradient echo and static signal suppression techniques. A pulse sequence for 3-D volume MR angiography is shown in Figure 5.25. The sequence is based on the 2-D planar

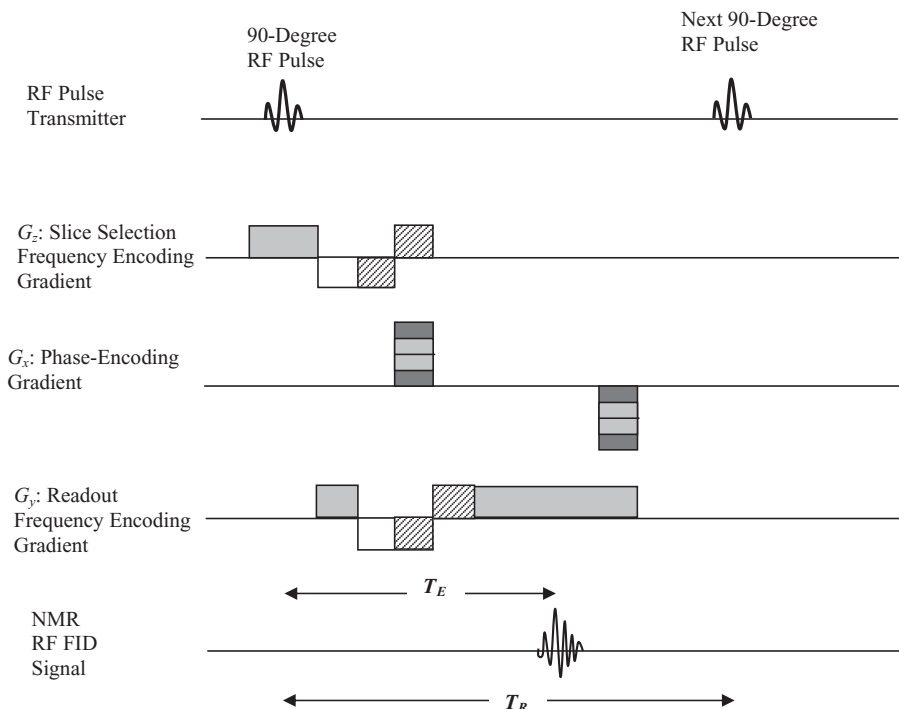


Figure 5.25 Gradient echo-based MR pulse sequence for 3-D MR volume angiography.

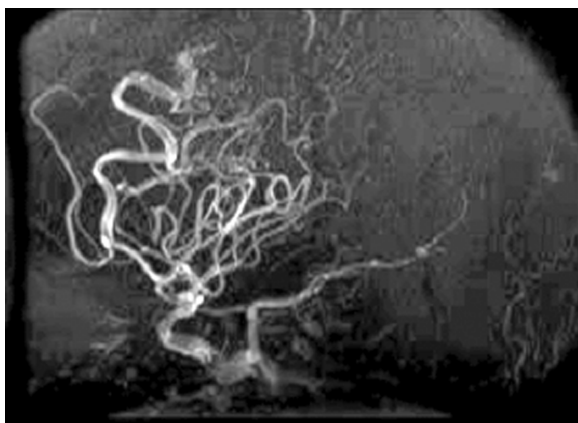


Figure 5.26 An MR angiography image.

imaging method and is repeated for the number of slices and the number of steps used in the phase encoding (3–7). The hatched regions in the gradient pulses provide necessary fields to compensate for phase sensitivity of the flow. An MR angiogram image is shown in Figure 5.26.

5.5. FMRI

Neural activity-based functions are critical for the survival of human beings as well as animals. For example, central and peripheral nervous systems of the human body contains hundreds of billions of neuronal cells that form different neural tissues in the brain and other parts of the body. Electrical signals or impulses such as action potentials are generated by neuronal cells in neural tissue for the proper physiological functioning of the body. The central nervous system involving the brain and spinal cord performs complex functions based on integration, generation, and transmission of electrical impulses. Neuronal cells generate electrical impulses in response to synaptic integration or sensory stimulations and consume oxygen in this process. Oxygenated hemoglobin molecules provide oxygen to enable cellular functions. As a neural tissue is stimulated for neural activity (firing of action potentials), oxygen is rapidly consumed by the cells, resulting in a decrease in the oxygen level in the blood. As the cells continue to demand oxygen for their functions, more oxygenated hemoglobin cells are rapidly needed, causing an increase in local blood flow. This phenomenon of increased blood flow and volume for high neural activity is known as hemodynamic response because of which the oxygenation level in the local region is increased as the blood flow is increased. Thus, the physiological functions of neural tissue such as that of the brain can be examined through its hemodynamic response, as neural activity can be representatively translated into increase of local blood flow and volume, which in turn shows an increase in oxygenation level. fMRI imaging methods measure blood oxygen level during sensory stimulation or any task that causes a specific neural activity. For example, visual or auditory stimulation, finger movement, or a cognitive task can cause neural activities in specific parts of cortical structures in the brain, causing increased cerebral blood flow. The blood oxygen level, or, simply put, blood flow, during neural stimulation is considered strongly correlated with glucose metabolism of the tissue. The neural activities or functions can be examined through blood oxygen level measurement by fMRI using blood oxygenated level dependent (BOLD) contrast (8, 9).

It is well known that oxygenated hemoglobin (HbO_2) is diamagnetic while deoxygenated hemoglobin (Hb) is paramagnetic. Thus, magnetic susceptibility is increased with the increase in oxygenated hemoglobin. This leads to an increase in MR signal with the increase in oxygen level in the blood or blood flow. This is effectively measured by BOLD imaging sequence. A reduction of the relative de-oxy-hemoglobin concentration due to an increase of blood flow and hence increased supply of fresh oxy-hemoglobin during neural activity is measured as an increase in T_2 or T_2 weighted MR signals. The difference in MR signals through BOLD in stimulated condition than the normal (or baseline) situation is usually very small. Therefore, the stimulation (or task) has to be repeated several times and MR signal measurements are taken through the repetition of BOLD sequence. The brain is scanned at a lower resolution with a fast pulse sequence such as gradient echo. Statistical correlation methods are applied to determine the specific area of the brain that reliably shows the significant difference in oxygen levels and is therefore considered to be involved in the respective neural activity. Figure 5.27

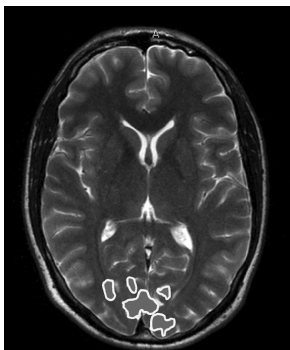


Figure 5.27 Functional magnetic resonance (fMRI) image of a human brain acquired through BOLD contrast sequence with visual stimulation. The activated areas in the visual cortex are outlined.

shows an MR image of a human brain with BOLD contrast activation areas in the visual cortex region that resulted from the visual stimulation task during imaging.

5.6. DIFFUSION IMAGING

As MRI uses hydrogen protons for creating FID signal to reconstruct images of proton density as well as spin-lattice and spin-spin relaxation parameters, specialized imaging pulse sequences can be designed to follow water molecules involved in diffusion around a cell. It is interesting to note that a neuronal cell in the neural tissue has a cell body known as soma with a dendrite tree carrying synaptic junctions for integration of electrical signals from other neurons, and a long axon that delivers the electrical signal to other neuronal synapses once the output action potential or impulse is generated by the cell. The cell uses a permeable membrane for ionic transport to modify its electrical potential to generate, receive, and transmit electrical signal. The biochemical functions of the membrane of the cell body and axon involves water diffusion (10–13). The water molecules can be tracked by diffusion-weighted MRI pulse sequences to characterize neural tissue. Neural tissue (such as brain tissue) in living beings is categorized largely into two categories: (1) gray matter containing cell bodies, and (2) white matter containing nerve fibers (axons with the protective myelin sheath that speeds up electrical transmission through the axon). It is clear that different regions of neural tissue (such as brain cortex) are interconnected through axonal pathways involving a huge number of synaptic junctions. A human body is believed to have as many as 300 billion neurons with several hundreds of trillions of synaptic junctions. It is important to image neural tissue characterizing gray and white matters for physiological functions such as water diffusion in the diagnosis, treatment, and rehabilitation of neurological disorders such as Parkinson's, Alzheimer's, and diseases involving loss of neural functions. DWI and DTI allow *in vivo* measurement of diffusivity of water molecules in the neural tissue.

In the diffusion process, water molecules spread out over time that is represented by Brownian motion. The displacement of diffused molecules can be modeled as an anisotropic Gaussian distribution along a given spatial axis such that the spread of the position of molecules after a time T along a spatial axis x can be represented with a variance of

$$\sigma_x^2 = 2DT \quad (5.26)$$

where D is diffusion coefficient in the tissue.

The directional displacement of diffused molecules is parameterized by the diffusion tensor. The diffusion tensor allows computation of diffusion anisotropy (directional activity) through the analysis of underlying eigenvalues of each voxel tensor field. The diffusion model assumes homogeneity and linearity of the diffusion within each image voxel. Axonal structure covered with myelin sheath, as shown in Figure 5.28, facilitates the diffusion of the water molecules preferentially along the direction of axons, providing anisotropic diffusion in the white matter. However, the gray matter lacks a specific orientation and therefore accounts for relatively isotropic diffusion.

The DTI through a specialized MRI pulse sequence provides information about the cellular organization in the tissue factor based on the state of the membrane permeability, myelination, compactness and axonal packing structure. DTI pulse sequence utilizes motion probing gradients (MPG) to examine the motion of water molecules in the diffusion process in a specific direction. As the data are collected while applying MPG in different directions, a diffusion tensor matrix is obtained and eigenvalues are computed to determine an anisotropy factor known as fractional anisotropy (FA), along with the diffusion magnitude and direction. DTI is performed with the application of MPGs in multiple gradient directions (e.g., 6 or more) to compute the diffusion tensor. In diffusion weighted imaging (DWI), three gradient directions are used to estimate the trace of the diffusion tensor or average diffusivity within each voxel.

Figure 5.29 shows a DWI/DTI pulse sequence for MRI. The pulse sequence is similar to spin-echo pulse sequence except that it uses two additional gradient pulses before and after 180-degree RF pulse to detect the motion of diffused molecules. For a faster scan, EPI pulse sequence can be used with two gradient pulses in a similar way. These two gradients are called motion probe gradients MPGs.

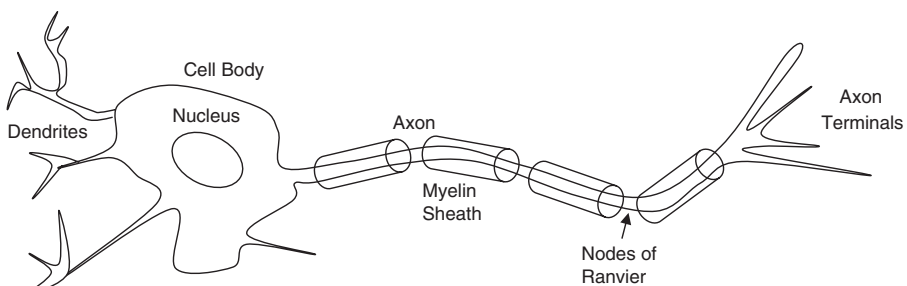


Figure 5.28 A schematic diagram of a neuron cell structure.

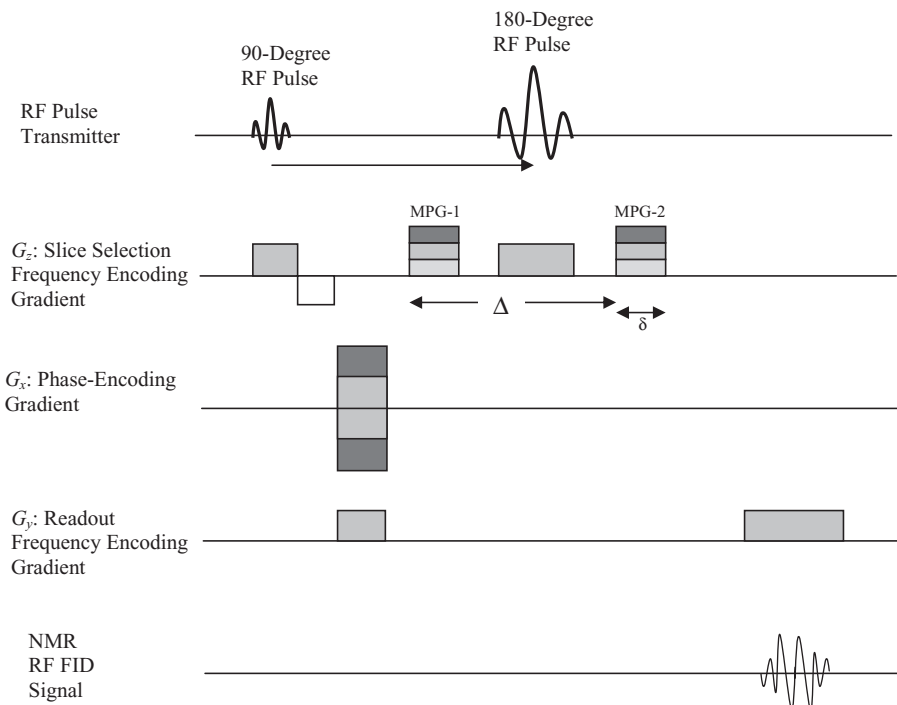


Figure 5.29 A DWI/DTI pulse sequence for MR diffusion imaging.

MPGs can be applied in any combination of predetermined directions to detect molecules diffusing in different directions. The first gradient pulse of MPG that is applied before the 180-degree RF pulse dephases the protons of water molecules, while the second gradient pulse in the same direction but with opposite polarity rephases their spins with respect to their displacement. In Figure 5.29, two gradient pulses of MPG each of δ duration are applied with Δ time difference. If the protons have moved between the times of application of these two gradient pulses, the rephasing does not take place completely resulting in the loss of signal. If the protons are stationary and do not move between the two gradient pulses, they are rephased with the spin-echo cycle and therefore yield a higher intensity signal. Thus, for healthy tissue with water diffusion, the MR FID signal is decreased while the tissue with trapped-in water molecules (as in the case of swelling of damaged tissue), the MR FID signal is increased. Let us assume that S and S_0 , respectively, represent MR FID signal intensities with and without diffusion weighting, then for a pulse sequence shown Figure 5.29, it can be shown as (14):

$$S = S_0 e^{-\gamma^2 G^2 \delta^2 (\Delta - \delta/N) D} \quad (5.27)$$

where γ is the gyromagnetic ratio, D is diffusion coefficient, and G is the strength of two MPG gradients each with δ duration separated by Δ applied in N spatial directions (e.g., for DWI imaging three spatial directions, x , y , and z , are used).

Equation 5.27 can be simply written as:

$$S = S_0 e^{-bD}$$

$$\text{with } b = \gamma^2 G^2 \delta^2 (\Delta - \delta / N) D \text{ providing } D = \frac{1}{b} \ln \frac{S}{S_0}. \quad (5.28)$$

It should be noted that D is a scalar quantity (average diffusivity) in case of DWI but is a tensor in case of DTI data. For example, if MPGs are applied with $u_x = (1, 0, 0)$; $u_y = (0, 1, 0)$; $u_z = (0, 0, 1)$ directions, a 3×3 tensor can be represented as

$$D = (u_x, u_y, u_z) \begin{bmatrix} D_{xx} & D_{xy} & D_{xz} \\ D_{yx} & D_{yy} & D_{yz} \\ D_{zx} & D_{zy} & D_{zz} \end{bmatrix} \begin{pmatrix} u_x \\ u_y \\ u_z \end{pmatrix}. \quad (5.29)$$

While the vector \bar{U} can be extended with a higher number of directions in which motion probe gradients are applied to collect the data, the tensor matrix is symmetric along the diagonal for which eigenvalues λ_1 , λ_2 , λ_3 and trace of $[D]$ can be computed as

$$\bar{\Lambda} = \begin{bmatrix} \lambda_1 & & \\ & \lambda_2 & \\ & & \lambda_3 \end{bmatrix} \quad (5.30)$$

$$\begin{aligned} \text{trace}[D] &= D_{xx} + D_{yy} + D_{zz} \\ &= \lambda_1 + \lambda_2 + \lambda_3. \end{aligned} \quad (5.31)$$

It should be noted that trace of $[D]$ is a scalar quantity providing diffusion weighted (DWI) images. Figure 5.30 shows an axial slice of DWI MR image of the brain with acute stroke. The medial cerebral artery (MCA) watershed infarction can be seen in the image.

In case of DTI data analysis, each eigenvalue is compared. If they are similar to each other for a given voxel, the voxel is considered belonging to the gray

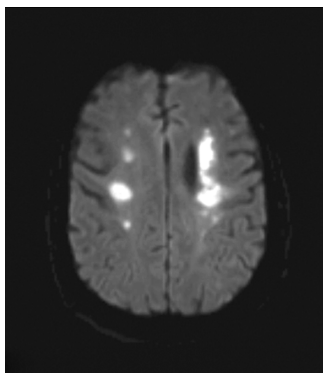


Figure 5.30 A diffusion weighted image (DWI) MR image of the brain with middle cerebral artery (MCA) watershed infarction.

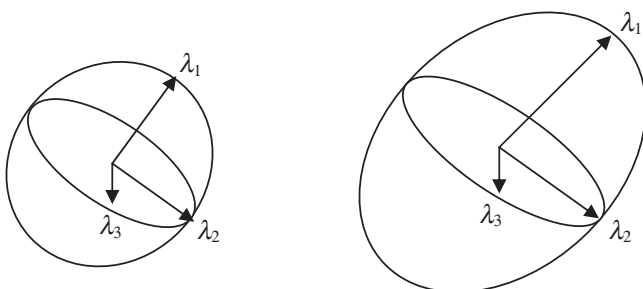


Figure 5.31 A schematic diagram of eigenvalue analysis for isotropic diffusion ($\lambda_1 \approx \lambda_2 \approx \lambda_3$) representing a gray matter voxel at the left, and anisotropic diffusion in the direction of λ_1 while $\lambda_1 > \lambda_2 > \lambda_3$ representing a white matter voxel at the right.

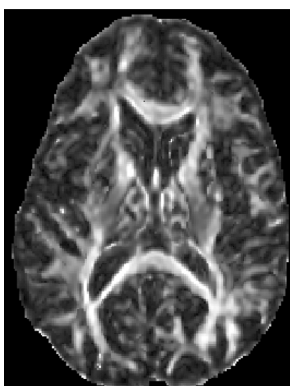


Figure 5.32 A color axial fiber orientation map of a diffusion tensor image (DTI) of a human brain in three eigenvector directions, x , y , and z , coded, respectively, in red, green, and blue colors.

matter (as there is no specific directional sensitivity in the data), but if they are different and can be arranged in a descending order, the diffusion directional sensitivity is determined in the direction of largest value of eigenvalue λ_1 as shown in Figure 5.31.

In case of anisotropic diffusion related to white matter of the neural tissue, FA is computed as

$$FA = \frac{1}{\sqrt{2}} \sqrt{\frac{(\lambda_1 - \lambda_2)^2 + (\lambda_2 - \lambda_3)^2 + (\lambda_3 - \lambda_1)^2}{\lambda_1^2 + \lambda_2^2 + \lambda_3^2}}. \quad (5.32)$$

The FA values as assigned to each voxel can be used to code connectivity among the voxels. Also, the FA values can be used in estimation of white matter tract orientations to show connectivity in white matter tractography (13, 14). A color-coded FA map of an axial brain image in three eigenvector directions, x , y , and z , coded, respectively, in red, green, and blue colors, is shown in Figure 5.32.

DWI/DTI show a great potential in diagnosis and treatment evaluation of diseases that disrupt normal organization and integrity of cerebral tissue such as

multiple sclerosis, strokes, tumors, Parkinson's and Alzheimer's disease. DTI is useful to study diseases of the white matter and connectivity of brain pathways. Patients with attention deficit hyperactivity disorder (ADHD) have been observed with abnormal fiber pathways in frontal cortex, basal ganglia, and cerebellum through DTI.

5.7. CONTRAST, SPATIAL RESOLUTION, AND SNR

The contrast in MR images comes from the differentiation of MR signal with respect to spin (proton) density, and T_1 and T_2 relaxation times. One of the major advantages of MRI is its sensitivity to soft tissue contrast. The actual contrast-to-noise ratio depends on the data collection method (pulse sequence or spatial sampling and signal averaging), imaging parameters (strength of magnetic field, spin density, T_1 and T_2 relaxation times, coil sensitivity) and any flow as applicable. Table 5.1 shows spin-density and relaxation time parameters for specific tissues. The faster scans such as single-shot EPI may not provide good contrast in the image as the data collection process compromises signal intensity with spatial sampling in a single cycle. In general, the contrast between two specific tissues can be estimated by the difference of respective signal intensities that are determined through the applied imaging pulse sequence as

$$S = k\rho \left(1 - e^{-\frac{T_R}{T_1}} \right) \left(e^{-\frac{T_E}{T_2}} \right) \quad \text{for spin-echo imaging pulse sequence.} \quad (5.33)$$

$$S = k\rho \left(\left(1 - 2e^{-\frac{T_I}{T_1}} \right) + e^{-\frac{T_R}{T_1}} \right) \left(e^{-\frac{T_E}{T_2}} \right) \\ \text{for inversion recovery (180-90-180) imaging pulse sequence.} \quad (5.34)$$

$$S = k\rho \frac{\left(1 - e^{-\frac{T_R}{T_1}} \right) \sin \theta \left(e^{-\frac{T_E}{T_2^*}} \right)}{\left(1 - \cos \theta e^{-\frac{T_R}{T_1}} \right)} \quad \text{for gradient echo imaging pulse sequence.} \quad (5.35)$$

where S is the signal intensity of FID in frequency domain, ρ is spin density, and k is a proportionality constant.

Spectral response of various tissues provides more dispersion at higher field strengths. It means that spectral peaks are better separated at higher field strengths and therefore certain lesions such as gray matter lesions in brain images can be better seen. It should also be noted that the SNR is significantly improved with higher field strength. However, higher field strength also increases T_1 relaxation time, which decreases overall contrast sensitivity because of the saturation effect in spin-lattice magnetization.

To improve the contrast of vascular structures, a paramagnetic contrast agent such as gadolinium (Gd) can be used to change the susceptibility of the net

magnetization vector. Such a paramagnetic contrast agent reduces T_1 relaxation time and therefore increases the signal intensity of T_1 -weighted images. As the contrast agent is injected in the vascular system, MRI is performed with the appropriate pulse sequence. MR angiography is a good example of MR contrast imaging. Gd-enhanced T_1 -weighted MR brain imaging is often used in diagnostic radiology.

There are several sources of noise and field inhomogeneities that cause artifacts and affect tissue contrast in MR images. Among them, the most prominent are RF noise, field inhomogeneities, motion, and chemical shift. RF shields are used to prevent external signals into RF coil. However, any failure in RF shield may cause bright artifacts such as spots or lines in the image due to RF noise. Nonuniformity of the external magnetic field and gradient coils can cause artifacts in the reconstructed image as the spatial frequency and phase encodings are adversely affected. Motion artifacts such as blurring and the appearances of ghost edges are caused by the motion of the tissue due to patient's movements or breathing during imaging.

Under an external magnetic field, each atom in the molecular structure of the tissue experiences its own small magnetic field (due to the circulation of electrons) in the direction opposite to the external magnetic field. Thus, the effective field strength at each nucleus varies depending on the molecular bonding and structure in the surrounding tissue. The chemical shift of a nucleus is determined as the deviation of its effective resonance frequency in the presence of other nuclei from a standard reference without any other nuclei with their local magnetic fields present. The chemical shift δ is expressed in ppm and computed as

$$\delta = \frac{(\omega - \omega_{ref}) \times 10^6}{\omega_{ref}}. \quad (5.36)$$

It can be seen from Equation 5.35 that chemical shift is proportionally impacted by the strength of external magnetic field that determines the Larmor frequency. It is also inversely proportional to the sampling rate in the direction of frequency encoding. Thus, chemical shifts affecting the Larmor frequency distribution, and therefore signal localization, cause artifacts in the presence of other nuclei in the tissue such as fat and water.

The SNR of a tissue in an image is the ratio of the average signal for the tissue to the standard deviation of the noise in the background of the image. In addition to the parameters above, SNR depends on signal acquisition methods and can be improved by signal averaging. With the assumption of a random noise in signal acquisition, the increase in SNR is proportional to the square root of number of images averaged. However, such image averaging to improve SNR is done at the expense of imaging time, which is often not a practical solution.

In conclusion, MRI is a relatively a noninvasive imaging method and uses no external radiation. It provides high-resolution multicontrast images due to its inherent capability of multiparameter signal acquisition methods that can be adopted and tuned to the imaging requirements with respect to pathology. Recent advances in functional and diffusion imaging have opened new doors to complex potential applications in neuroimaging.

5.8. EXERCISES

- 5.1. What is the principle of magnetic resonance imaging (MRI)? Which imaging modality would you choose to obtain images with better soft-tissue contrast? Explain your answer.
- 5.2. Under the external magnetic field strength of 1.5T, what is the Larmor frequency for the nuclei: (i) ^1H , (ii) ^{23}Na , and (iii) ^{31}P ?
- 5.3. What are the major advantages of MRI?
- 5.4. Explain Bloch's equation with respect to a rotating magnetization frame for longitudinal and transverse magnetization vectors.
- 5.5. Describe the longitudinal and transverse magnetization decays. How are these decays used in MRI?
- 5.6. What are the characteristic features of RF coils used in MRI?
- 5.7. Explain the various factors influencing the MR signal intensity and its shape.
- 5.8. How are the longitudinal and transverse relaxation times computed?
- 5.9. Let us assume that a tissue has a spin-lattice relaxation time of 100ms. How long will it take for the longitudinal relaxation time to recover by 90%? (Consider the initial net magnetization vector to be zero.)
- 5.10. Let us assume that a tissue has a spin-spin relaxation time of 100ms. Find the time of transverse magnetization vector to decay to 30% of its initial value.
- 5.11. Describe a general spin-echo imaging pulse sequence. What are the major issues in implementing it for 3-D imaging?
- 5.12. Describe fast EPI imaging sequence for 3-D imaging. What are its advantages and disadvantages over spin-echo pulse sequence?
- 5.13. Describe a gradient echo imaging pulse sequence with the explanation of sampling in the k -space. What are its advantages and disadvantages over EPI pulse sequence?
- 5.14. Draw a timing diagram for an inversion recovery imaging sequence that uses a 90-FID sequence to detect the signal present T_1 after the inversion (180-degree) pulse.
- 5.15. How are the activation areas determined in fMRI?
- 5.16. What T_E should be used to maximize contrast between two tissues with spin-spin relaxation times of 30 and 40ms in spin-echo pulse sequence?
- 5.17. What is diffusion imaging? Describe an imaging pulse sequence and discuss its differences from flow imaging.
- 5.18. What is the difference between DWI and DTI?
- 5.19. What is fractional anisotropy and how is it computed?
- 5.20. Display in MATLAB the axial MR brain images with a stroke. Display proton density, T_1 -weighted, T_2 -weighted, and DWI images in separate windows. Compare and contrast the spatial resolution of each image with respect to lesions, white matter, gray matter, and CSF space.

5.9. REFERENCES

1. J.T. Bushberg, J.A. Seibert, E.M. Leidholdt, and J.M. Boone, *The Essentials of Medical Imaging*, Williams & Wilkins, Philadelphia, 1994.
2. Z.H. Cho, J.P. Jones, and M. Singh, *Fundamentals of Medical Imaging*, John Wiley & Sons, New York, 1993.
3. Z. Liang and P.C. Lauterbur, *Principles of Magnetic Resonance Imaging*, IEEE Press, Piscataway, NJ, 2000.
4. M.H. Lev and F. Hochberg, “Perfusion magnetic resonance imaging to assess brain tumor responses to new therapies,” *J. Moffit Cancer Cent.*, Vol. 5, pp. 446–450, 1998.
5. D.D. Stark and W.G. Bradley, *Magnetic Resonance Imaging*, 3rd Edition, Mosby, New York, 1999.
6. F. Schmitt, M.K. Stehling, and R. Turner (Eds), *Echo Planar Imaging Theory, Techniques and Applications*, Springer-Verlag, Berlin, 1998.
7. K.K. Shung, M.B. Smith, and B. Tsui, *Principles of Medical Imaging*, Academic Press, San Diego, CA, 1992.
8. C.T.W. Moonen and P.A. Bandettini, *Functional MRI*, Springer-Verlag, Berlin, 2000.
9. P. Jezzard, P.M. Mathews, and S.M. Smith (Eds), *Functional Magnetic Resonance Imaging: An Introduction to Methods*, Oxford University Press, Oxford, 2001.
10. M.E. Moseley, J. Kucharczyk, J. Mintorovitch, Y. Cohen, J. Kurhanewicz, N. Derugin, H. Asgari, and D. Norman, “Diffusion-weighted MR imaging of acute stroke: Correlation with T_2 -weighted and magnetic susceptibility-enhanced MR imaging in cats,” *AJNR Am. J. Neuroradiol.*, Vol. 11, No. 3, pp. 423–429, 1990.
11. P.J. Basser, J. Mattiello, et al., “Estimation of the effective self-diffusion tensor from the NMR spin echo,” *J. Magn. Reson. B*, Vol. 103, No. 3, pp. 247–254, 1994.
12. C.H. Sotak, “The role of diffusion tensor imaging in the evaluation of ischemic brain injury—a review,” *NMR Biomed.*, Vol. 15, No. 7–8, pp. 561–569, 2002.
13. M.E. Moseley, J. Kucharczyk, J. Mintorovitch, Y. Cohen, J. Kurhanewicz, N. Derugin, H. Asgari, and D. Norman. Diffusion-weighted MR imaging of acute stroke: correlation with T_2 -weighted and magnetic susceptibility-enhanced MR imaging in cats. *AJNR Am J Neuroradiol*, Vol. 11, pp. 423–429, 1990.
14. D.S. Kim and I. Ronen, “Recent advances in diffusion magnetic resonance imaging,” in A.P. Dhawan, H.K. Hunag, and D.S. Kim (Eds), *Principal and Advanced Methods in Medical Imaging and Image Analysis*, World Scientific Press, Singapore, pp. 289–309, 2008.